nature chemical engineering

Review article

https://doi.org/10.1038/s44286-023-00009-x

Multi-scale physics of bipolar membranes in electrochemical processes

Received: 17 August 2023

Accepted: 14 November 2023

Published online: 11 January 2024

Check for updates

Justin C. Bui[1,2] ✉, Eric W. Lees[3], Daniela H. Marin[4], T. Nathan Stovall[3,5], Lihaokun Chen[6], Ahmet Kusoglu[3], Adam C. Nielander[7], Thomas F. Jaramillo[4,7], Shannon W. Boettcher[6], Alexis T. Bell[1,2] & Adam Z. Weber[2,3] ✉

Bipolar membranes (BPMs) enable control of ion concentrations and fluxes in electrochemical cells suitable for a wide range of applications. Here we present the multi-scale physics of BPMs in an electrochemical engineering context and articulate design principles to drive the development of advanced BPMs. The chemistry, structure, and physics of BPMs are illustrated and related to the thermodynamics, transport phenomena, and chemical kinetics that dictate ion and species fluxes and selectivity. These interactions give rise to emergent structure–property–performance relationships that yield design criteria for BPMs that achieve high permselectivity, durability, and voltaic efficiency. The resulting performance trade-offs for BPMs are presented in the context of emerging applications in energy conversion or storage, and environmental remediation. By connecting the fundamental physical phenomena in BPMs to device-level performance and engineering, we aim to facilitate the development of next-generation BPMs for sustainable electrochemical processes.

Bipolar membranes (BPMs) are a class of ion-conductive polymers (ionomers) composed of two layers with fixed charges adhered to each other, often with a catalyst layer (CL) between them (Fig. 1a)[1,2]. One ionomer layer, the cation-exchange layer (CEL), contains fixed negative charges. The other layer, the anion-exchange layer (AEL), contains fixed positive charges. BPMs have two operating modes in electrochemical systems: forward and reverse bias (Fig. 1a)[3].

In forward bias, cations and anions are transported towards the AEL/CEL interface, respectively, where they recombine. In reverse bias, electric fields (up to 10^8 V m^{-1}) and catalytic effects within the AEL/CEL interface drive the breakdown of polarizable species (for example, water or acid) into cations and anions that are transported into the CEL and AEL, respectively[4–6]. In both operating modes, the fixed charges on the ionomer limit crossover of co-ions (ions with the same charge as the fixed charges) through the BPM by electrostatic repulsion (Donnan exclusion). Conversely, counter-ions (ions with the opposite charge as the fixed charges) are selectively partitioned and transported[7]. The ability for BPMs to control and sustain different local chemical environments and drive the dissociation or formation of chemical species with an applied voltage enables the interconversion of chemical- and electrical-potential gradients, making BPMs unique solutions for electrochemical applications[1,8].

Since their invention in 1956[9], BPMs have been used in small-scale processes in the food industry[10] and to produce acid and base[11]. BPMs have also been demonstrated for chloro-alkali processes[12] and other electrochemical devices that require pH control and ion selectivity. However, there has been a renaissance over the past decade due to improvements in ionomers, the advent of low-cost renewable electricity, and growing recognition of value in controlling local reaction environments for selectivity, efficiency, and cost. Additionally, the

[1]Department of Chemical and Biomolecular Engineering, University of California, Berkeley, CA, USA. [2]Liquid Sunlight Alliance, Lawrence Berkeley National Laboratory, Berkeley, CA, USA. [3]Energy Technologies Area, Lawrence Berkeley National Laboratory, Berkeley, CA, USA. [4]Department of Chemical Engineering, Stanford University, Stanford, CA, USA. [5]Department of Chemistry, University of California, Berkeley, CA, USA. [6]Department of Chemistry and the Oregon Center for Electrochemistry, University of Oregon, Eugene, OR, USA. [7]SUNCAT Center for Interface Science and Catalysis and Liquid Sunlight Alliance, Menlo Park, CA, USA. ✉e-mail: justin_bui@berkeley.edu; azweber@lbl.gov

https://doi.org/10.1038/s44286-023-00009-x

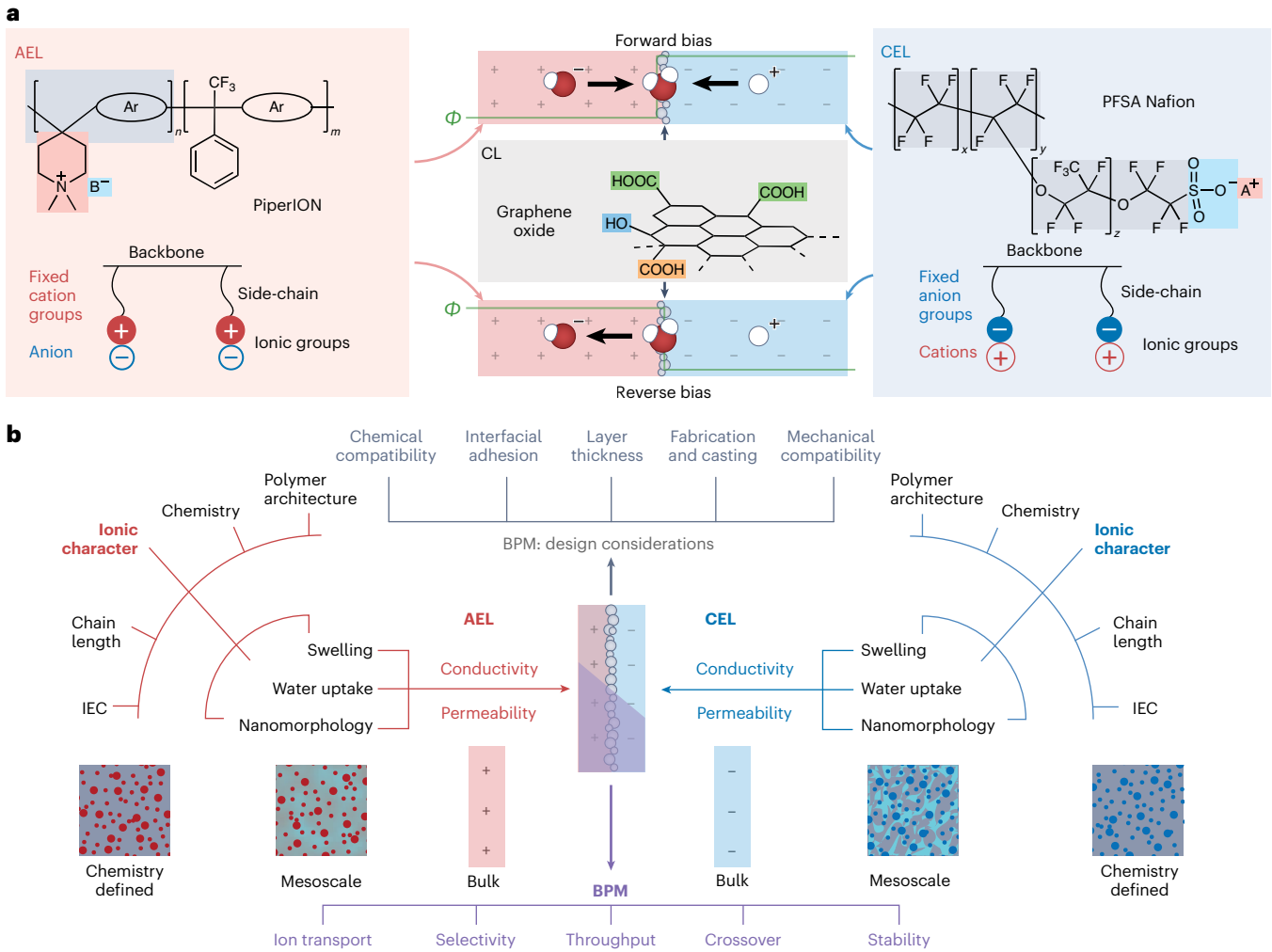

Fig. 1 | Overview of BPM design considerations. a, Schematic of BPMs operating in forward and reverse bias. Chemical structure of the AEL (left), CL (middle, sometimes referred to as the interfacial layer), and CEL (right). **b**, Schematics of BPMs and chemical and physical properties at each scale and how they impact design and physical observables. The materials and structure of the BPM shown are examples; the best-performing BPMs demonstrated today utilize a Nafion CEL, a PiperION AEL, and a nanoparticle catalyst layer[13,14]. Other polymer chemistries, such as hydrocarbon CELs, or junction morphologies, such as interwoven[138] and electrospun[59], can appear in BPMs as well.

development of advanced interfacial catalysts has significantly reduced BPM energy requirements[13–15] that have long been an important contributor to cost precluding their industrial application[16], with recent demonstrations exhibiting performance close to the thermodynamic minimum even at high current densities approaching 1 A cm^{-2} (refs. 13,14,17). However, an untapped opportunity exists to leverage engineering approaches to optimize BPM systems. From the kinetics of dissociation–recombination within the nanoscale catalyst layer, to the efficient management of mesoscale ionic transport and material degradation, to the macroscale optimization of integrated assemblies, multi-scale understanding can help link the properties of materials and interfaces to BPM system performance (Fig. 1b).

In this Review, we present challenges and opportunities in BPM development. We briefly discuss the physicochemical properties of ionomers. Next, we discuss BPM physics in terms of thermodynamics, transport phenomena, and chemical kinetics, where structure–property–performance relationships are presented to provide guidelines for BPM development and integration into cells and reactors. These principles contextualize performance of three emerging BPM applications: (1) water electrolysis and CO_2 reduction (CO_2R), (2) flow batteries and fuel cells, and (3) environmental remediation. Present challenges in BPM deployment at-scale are also discussed, ending with an outlook on the opportunities for chemical-engineering insight to help improve the durability, performance, and scale of BPM systems.

Chemical and physical properties of ion-conducting polymers

The ionomers used in BPMs are solid-polymer electrolytes wherein fixed-charge groups covalently attached to the polymer matrix enable selective uptake and transport of counter-ions. Ionomers are classified in terms of counter-ion identity: AELs conduct anions and CELs conduct cations. The ionomer's chemical and physical structures (Fig. 1) result in a nano- and meso-morphology responsive to the external environment, facilitating ion hydration while maintaining mechanical stability[18].

The chemical structure of ionomers consists of long-chain polymer backbones with fixed-charged groups attached to either the side-chains, like in perfluorosulfonic acids (PFSAs), or the backbone itself, like in PiperION. Polar electrolytes solvate the charged groups, swelling the ionomer. The quantity of ionic groups in the polymer is termed the ion-exchange capacity (IEC), which is a measure of the moles of fixed-charge groups per unit mass of polymer. Structural factors also control ion transport, including nanostructure, confinement effects, and mesoscale morphology[15].

Typically, more hydrophobic ionomers like PFSAs possess phase-segregated domains, a hydrophobic backbone phase, and a

hydrophilic electrolyte phase, which results in nanoscale ordering and enhanced conductivity[19]. However, these are traditionally fluorinated materials (especially for CELs that are mainly PFSAs) for improved performance and durability[18]. Research is required to address the environmental implications of such polymers and develop suitable hydrocarbon-based replacements. Conversely, the majority of AELs are hydrocarbon based with more amorphous morphology due to their less-hydrophobic backbone (see different mesoscale morphologies in Fig. 1b). Although fluorinated ionomers are commonly used as the CEL in research-stage BPMs, fluorinated ionomers can be more expensive than certain hydrocarbon ionomers (although this depends on chemistry, processing and economies of scale). Hence, commercial BPMs commonly employ proprietary hydrocarbon resins, even for the CEL. Although Nafion is the prototypical research CEL due to its availability, BPMs with hydrocarbon CELs have demonstrated performance on par with Nafion-based BPMs[17,20].

The key performance properties of BPM ionomers are the individual layer thickness, IEC, and solvent uptake[18,21]. Generally, ionomers with larger IECs possess higher uptake of polar solvents due to the hydrophilic nature of the fixed-charge groups. Correspondingly, as the IEC increases, the ionomer becomes more conducive for ionic and polar solvent transport because the electrolyte phase is more strongly percolated. However, beyond a certain point, the ionomer becomes highly swollen with solvent, compromising its mechanical integrity. The opposite phenomenon occurs for non-polar solvents like hexanes: increasing IEC reduces uptake.

While a wealth of knowledge on the PFSAs has accumulated over the past few decades[18], structure–property relationships for AELs or hydrocarbon CELs are not well established[22]. Even more unexplored are the chemical and mechanical interactions between the AEL and CEL that give rise to emergent properties in BPMs. BPMs are a composite of two ion-exchange layers that can each possess varying properties, as well as an interface that can be engineered for improved adhesion. Hence, BPMs can potentially enable greater functionality, for example, using a thin CEL to accelerate transport with a thick AEL for improved mechanical stability[23].

The emergent properties of BPMs render these materials susceptible to different failure modes from what is observed in monopolar membranes. Strong physicochemical interactions between AELs and CELs improve overall stability[14,24]; however, unequal swelling (solvent uptake) and transport properties can cause BPM delamination[14]. Therefore, BPMs must be fabricated with chemically and mechanically compatible polymer layers. Resolving the physics that underlie the compatibility and interaction of oppositely charged polymers is a necessary focus of future studies.

Governing physics of BPMs

Thermodynamics

A major source of BPM complexity is the thermodynamic coupling between species—the local concentrations and properties of a single solvent or solute species can influence the behavior of all other components in the system. Complex partitioning of ions and solvent occurs within BPMs, wherein certain species are favored over others, and the local environment varies drastically from that of the bulk electrolyte (Fig. 2a)[18,25–27]. Ion and solvent partitioning between the external solution phase (α) and the membrane phase (δ) can be described by (electro) chemical equilibrium,

$$\tilde{\mu}_i^{\alpha} = \tilde{\mu}_i^{\delta} \tag{1}$$

where $\tilde{\mu}_i^{\delta}$ is the electrochemical potential of species i in membrane phase δ, defined below.

$$\tilde{\mu}_i^{\delta} - \tilde{\mu}_i^{\theta} = RT\ln\left(\frac{c_i}{c_{\text{ref}}}\right) + z_i F\Phi + \tilde{\mu}_i^{\text{ex},\delta} \tag{2}$$

where R is the ideal-gas constant, T is the absolute temperature, F is Faraday's constant, Φ is the ionic potential, and c_i and z_i are the concentration and valence of species i, respectively. $\tilde{\mu}_i^{\theta}$ is the standard-state electrochemical potential, defined as a pure liquid solvent containing non-interacting species (that is, ideal solution limit at a reference concentration of 1 M) and under no mechanical forces. The first term accounts for contributions due to ideal mixing; the second term describes explicit contributions from the electric field and is zero for uncharged species ($z_i = 0$); and the third term represents the excess free-energy contributions from nonideal interactions[28]. It should be noted that single-ion activities or concentrations are undefined and thus one needs to assume a reference species.

Under ideal conditions $\tilde{\mu}_i^{\text{ex},\delta}$, Donnan equilibrium applies, where the electrostatic potential change across the membrane/electrolyte interface ($\Delta\Phi_{\text{Donnan}}$) drives selective uptake or exclusion of ions into the BPM based solely on their charge (Fig. 2a, left). Donnan equilibrium predicts that all ions of the same charge partition equally and does not account for solvent uptake; hence, non-ideal interactions must be considered (Fig. 2a, middle and right)[25].

The speciation between absorbed species and solvent (for example, acid–base equilibria) are critical in BPMs—particularly the effects of water dissociation (WD) due to its prevalence as a solvent[21,29,30]:

$$H_2O_{(l)} \leftrightharpoons H^+_{(aq)} + OH^-_{(aq)} | K_w = 1\times10^{-14} \text{ at } T = 298\,\text{K} \tag{3}$$

The macroscopic equilibrium constants of WD (and other dissociation reactions) can depend on the local electric field through Onsager's second Wien effect, which is approximated by an exponential dependence[6,31,32],

$$K_w\left(|\bar{E} = -\bar{\nabla}\phi|\right) = K_w\left(|\bar{E}| = 0\right) \times f_{\text{eq}}(|\bar{E}|) \approx K_w(|\bar{E}| = 0) \times e^{\beta|\bar{E}|} \tag{4}$$

where $|\bar{E}|$ is the magnitude of the local electrostatic field, $f_{\text{eq}}(|\bar{E}|)$ is the functional dependence of the equilibria on the local electric field, and β is a semi-empirical parameter related to the dielectric properties of the dissociating molecule and its local environment. This phenomenon can best be understood as a lowering of the (local) free energy of dissociation due to the reorientation of a polarizable molecule under the presence of a large $|\bar{E}|$. While this framework is most commonly applied to water dissociation[6], it is applicable to any reaction where net charge is generated (for example, dissociation of buffering anions[30] or alcohols[33]). Correspondingly, this theory provides a framework to understand one possible role of electric fields on reaction chemistry, which is important to many chemical processes[34].

Species transport

BPM performance is dictated by the interplay between non-equilibrium reaction and transport processes[3,21,26,35]. These processes include: (1) transport of co- and counter-ions; (2) transport of solvent to and from the BPM junction; (3) dissociation of species; and (4) homogeneous reactions (Fig. 2b). Understanding species transport is necessary to resolve BPM performance including the origin of limiting current densities[36], co-ion leakage[21], and other phenomena.

There are two general frameworks for understanding transport in electrolyte solutions[37,38]. In the limit of small-ion and solute concentrations, dilute-solution theory is valid[26], which states that the diffusional flux of species i is directly proportional to its chemical-potential gradient and that convective flux is proportional to bulk velocity[26],

$$\bar{N}_i = -D_i c_i \bar{\nabla}\tilde{\mu}_i^{\text{ideal},\delta} + c_i\bar{v} = -D_i\bar{\nabla}c_i - \frac{z_i F}{RT}D_i\bar{\nabla}\Phi + c_i\bar{v} \tag{5}$$

where $\bar{N}_i$ represents the flux of species i, D_i is the diffusivity of species i in the solvent, and v is the bulk velocity. Note that the ion mobility above has been replaced by the diffusivity using Nernst–Einstein[37],

https://doi.org/10.1038/s44286-023-00009-x

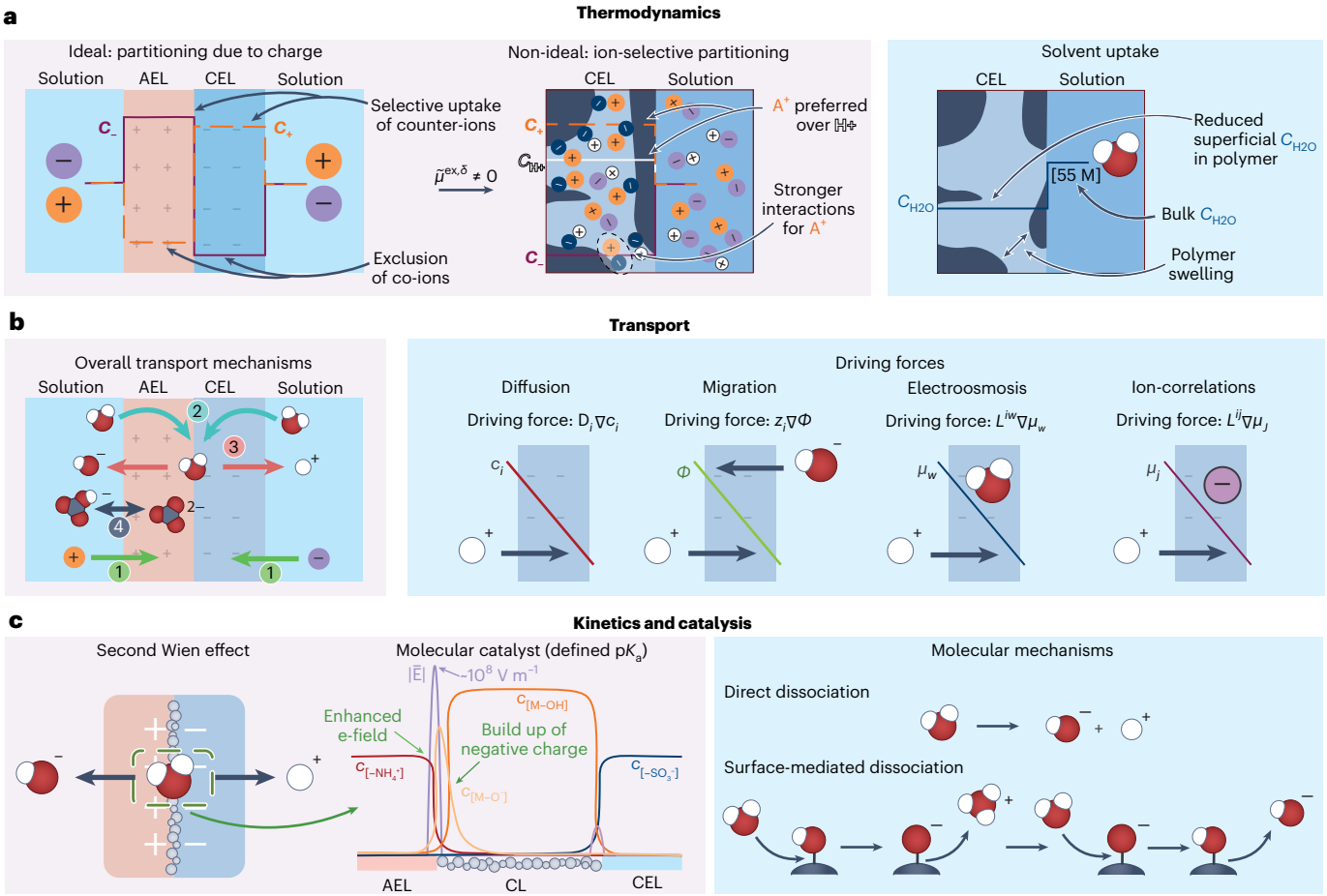

Fig. 2 | Overview of thermodynamics, transport phenomena, and kinetics in BPMs. a, Thermodynamics depicts the role of chemical potentials in dictating ion (left) and solvent (right) partitioning. c_i denotes the concentration of a given species i. A^+ represents a general alkali cation that is not H^+. **b**, Transport phenomena show the overall transport mechanisms (left) of (1) co-ion crossover, (2) water flux, (3) WD, and (4) homogeneous reactions, along with a detailed depiction of the driving forces that govern these overall mechanisms (right). **c**, Kinetics depicts the second Wien effect (left) and a cartoon of the surface species concentration and electric-field profiles in a BPM CL with well-defined pK_a, as well as proposed water-dissociation-mechanism schematics (right).

which applies at infinite dilution. Nearly all current reaction-transport models of BPMs use dilute-solution theory due to low current densities and concentrations[6,14,21,32,36,39]. Such models can predict rates of co-ion leakage, observable BPM properties (for example, conductivity[26,40]), and the fractional current densities carried by individual ions for BPMs operating <20 mA cm^{-2} in a variety of electrolytes[21].

Unfortunately, dilute-solution theory cannot resolve several phenomena that occur at high current densities[41] and with multiple species, where most industrial applications of BPMs must operate. This is because species–species interactions are neglected, for instance, water transport due to ion movement (electro-osmosis) can dramatically influence limiting-current densities[26,42,43], and similarly controls limiting WD behavior. Furthermore, ion crossover in BPM seawater electrolysis is attenuated at high current densities despite larger electromotive driving forces, which is hypothesized to be a result of frictional interactions between co-ions and generated H^+/OH^- (ref. 44).

Concentrated-solution theory starts with the Onsager framework[26,42,45–47], where the species flux is[48]

$$\bar{N}_i = -\sum_j L^{ij}\bar{\nabla}\tilde{\mu}_j + c_i\bar{v} \tag{6}$$

where L^{ij} is a transport coefficient that relates the flux of one species to the gradient in another species' chemical potential[37]. Concentrated-solution theory utilizes the correct number of measurable transport properties ($\frac{(n-1)n}{2}$), and the driving force accounts for non-ideal effects. This increase in rigor and complexity comes at a cost of significantly more knowledge needed to describe transport using concentrated-solution theory, and represents a parameterization challenge. Nonetheless, similar modeling work for cation exchange membranes (CEMs)[26] or polyelectrolyte solutions[48] provides a starting point for developing a comprehensive description of transport in BPMs.

Both concentrated- and dilute-solution theories can be integrated into conservation equations to couple transport with homogeneous reactions that occur throughout the BPM. The mass-conservation expression for species and solvent is

$$\bar{\nabla} \cdot \bar{N}_i = R_i \tag{7}$$

where R_i is a source term of generation or consumption of species i.

Charge conservation and separation in the BPM can be described by Poisson's equation[21],

$$\bar{\nabla} \cdot (\varepsilon\bar{E}) = F\sum_i z_i c_i \tag{8}$$

where ε is the local dielectric constant. Crucially, charge conservation defines the electric field that results from the applied voltage across the BPM and drives the second Wien effect.

Finally, the effects of energy dissipation and transport at the device level can be accounted for by including an energy balance. Temperature variations in BPM-containing electrochemical systems are likely to become important at high current densities where Joule and reaction heating induce temperature variations[3]. Modeling these temperature gradients is important because BPM performance and stability are temperature dependent as it impacts reaction rates[43,49], transport, swelling, and mechanical properties[18].

Reaction kinetics and catalysis

The kinetics of water dissociation and recombination in BPMs play a key role in defining device-level performance. For WD, most theories rationalizing the observed rates in BPMs are based on Onsager's second Wien effect[50]. In terms of kinetics, this framework states that the kinetic rate of a charged-species-generating reaction increases due to the large electric fields enhancing the separation of generated charges, which leads to an approximately exponential increase in the dissociation rate (that is, the rate constant increase is equivalent to the increase in the thermodynamic equilibrium constant in equation (4)). Conversely, the recombination rate is usually not strongly impacted by electric field because it is diffusion limited, which is consistent with molecular and quantum theories of the process[6].

The second Wien effect can explain observed increases in WD rates in uncatalyzed BPMs (that is, BPMs without a CL at the AEL/CEL interface), but it cannot solely explain the response of catalyzed BPMs. This is because the distance over which the electric potential drops is much larger in catalyzed BPMs (typically >100 nm), making the magnitude of the electric field too small to accelerate the rate of WD substantially. New theories and models that account for the modified local electric-field distribution through the AEL/CL/CEL interface are needed, and must also consider the various possible catalyzed reaction paths including possible protonation/deprotonation reactions on oxide WD catalysts[21,51]. This surface protonation/deprotonation is predicted to increase the local electric field in the CL and subsequently rate of WD[6,14,39,52]. For example, it was predicted[6] that a field buildup at the AEL/CL interface (Fig. 2c, left)[6,52] is why lower pK_a catalysts (MOH) are favorable due to their ability to generate additional negative charge (MO^-). This theory has been expanded[14], where a graphene oxide (GrOx) dissociation catalyst was modeled and compared with experimental data, revealing that protonation sites on GrOx possess various functionality for WD depending on their pK_a. Low pK_a sites deprotonate readily to screen the electric field, whereas high pK_a sites maintain their surface OH^- groups to provide active sites for a surface-mediated dissociation pathway (Fig. 2c, right). For catalysts that instead accept protons to form positively-charged species, lower pK_b is favorable, and the electric field forms at the CL/CEL interface rather than the AEL/CL interface[39].

Although the above framework is appropriate for WD on catalysts containing sites with well-defined pK_a values, these theories are likely inadequate for describing dissociation kinetics on metal-oxide catalysts, which do not have discrete pK_a values associated with well-defined functional groups. Instead they are better described as having a proton-absorption isotherm with an average proton binding strength and interaction term[53]. BPMs with optimal loadings of metal-oxide catalysts yield record voltaic efficiency[17], and have nearly linear current–voltage response instead of the more-exponential shape observed for uncatalyzed and GrOx-based BPMs[13,51]. Electronically conductive, or high dielectric, metal-oxide catalysts have much faster WD kinetics than electronically insulating catalysts, suggesting a key role in electric-field screening, where catalyst mobile electronic charge redistributes and cancels the electric field in the solid, thereby resulting in a stronger field directly outside of the particle. Coupled with an apparent activation energy independent of applied voltage, these results rationalize a new picture of WD catalysis, where the linear dependence of rate on voltage is caused by a build up of electric fields at the surface of each catalyst particle that increases the rate of WD by entropically reorientating water around each particle[13].

Metal-oxide catalysts also dramatically improve rates of H^+/OH^- recombination in forward-biased BPMs[15]. This is counterintuitive, because H^+/OH^- recombination is thought to be diffusion limited. This enhancement has been justified by invoking a surface-mediated recombination mechanism in which H^+ adsorbs on the catalyst surface to form protonated intermediates that react with OH^-, thus providing a faster alternative path compared with direct recombination in the bulk[15]. More work is needed to understand these possible mechanisms.

The above theories provide initial structure–property–performance relationships for interfacial catalysts, where surface properties, particle conductivity, and active area appear to be the most prominent predictors of catalyst performance[13,14,51]. Continuum theories have also enabled the simulation of the sharp gradients and local environments within the CL[14,21]. However, more advanced experimental techniques are needed to validate these predictions. Coupling theoretical descriptors from ab-initio approaches to the continuum scale with advanced spectroscopic techniques would be useful to resolve electric-field-enhanced catalysis and self-consistently describe observed behavior on molecular and metal-oxide catalysts used in BPMs.

Interpreting a BPM polarization curve

The electrochemical behavior of BPMs is often characterized using a four-probe through-plane electrochemical cell, where reference electrodes are placed on either side of the BPM submerged in either symmetric salt solutions or acid in contact with CEL and base in contact with AEL. The reference electrodes sense the difference in potential between them. Figure 3a depicts a BPM polarization curve with 1 M potassium acetate (KOAc) and 1 M sulfuric acid (H_2SO_4) contacting the AEL and CEL, respectively. There are four regions in the resulting polarization curve that result from the physical phenomena discussed above (Fig. 3b)[21,49]. First, is the negative current regime that is due to ion recombination (with positive current assigned to dissociation). Second, is the region where co-ion crossover dominates. Third, is electric-field-enhanced WD. Fourth, is where the maximum rates of water transport to the BPM junction yield an apparent limiting current. Co-ion crossover occurs in regions III and IV as well, but is the minority (<5%) contribution to current density in those regions.

Identifying each of these regimes is useful in resolving underlying and controlling phenomena. Figure 3c summarizes literature sensitivity analyses (that is, the observed effect of varying the value of a material or physical property on the electrochemical behavior in these regimes). The plots shown in Fig. 3c are simple schematic plots that depict the trends observed in observed polarization behavior upon changing properties of the BPM, electrolyte, or WD catalyst. In a case with non-buffering salts and negligible interface acid–base recombination, the open-circuit potential (OCP) is dictated by the applied pH gradient[54]. When buffer species transport through the BPM, the OCP is dictated by the p$K_{a/b}$ of the buffer[35]. The current for recombination is dictated by the presence of a catalyst, its loading, morphology, distribution, and active area, along with the ionomers' transport properties (Fig. 3c(i)). Thinner membranes or those possessing higher IECs enable improved performance in mass-transfer regimes (Fig. 3c(iv)), but also lead to an increase in deleterious co-ion leakage (Fig. 3c(ii)). For more detailed information on the relationship between ionomer properties and structure, we refer the reader to review articles focused on monopolar membranes[18,55,56]. Behavior in the WD regime is dictated primarily by the catalyst properties[39,51,57] and to a lesser extent the ionomer properties[21] (Fig. 3c(iii)).

An alternative measurement of BPM properties can be made in a membrane-electrode assembly (MEA), similar in construction to a pure-water-fed electrolyzer or fuel cell. The advantage of these architectures is that OH^- and H^+ are the only mobile ions, thereby making it more straightforward to resolve the basic mechanisms of WD in BPMs.

https://doi.org/10.1038/s44286-023-00009-x

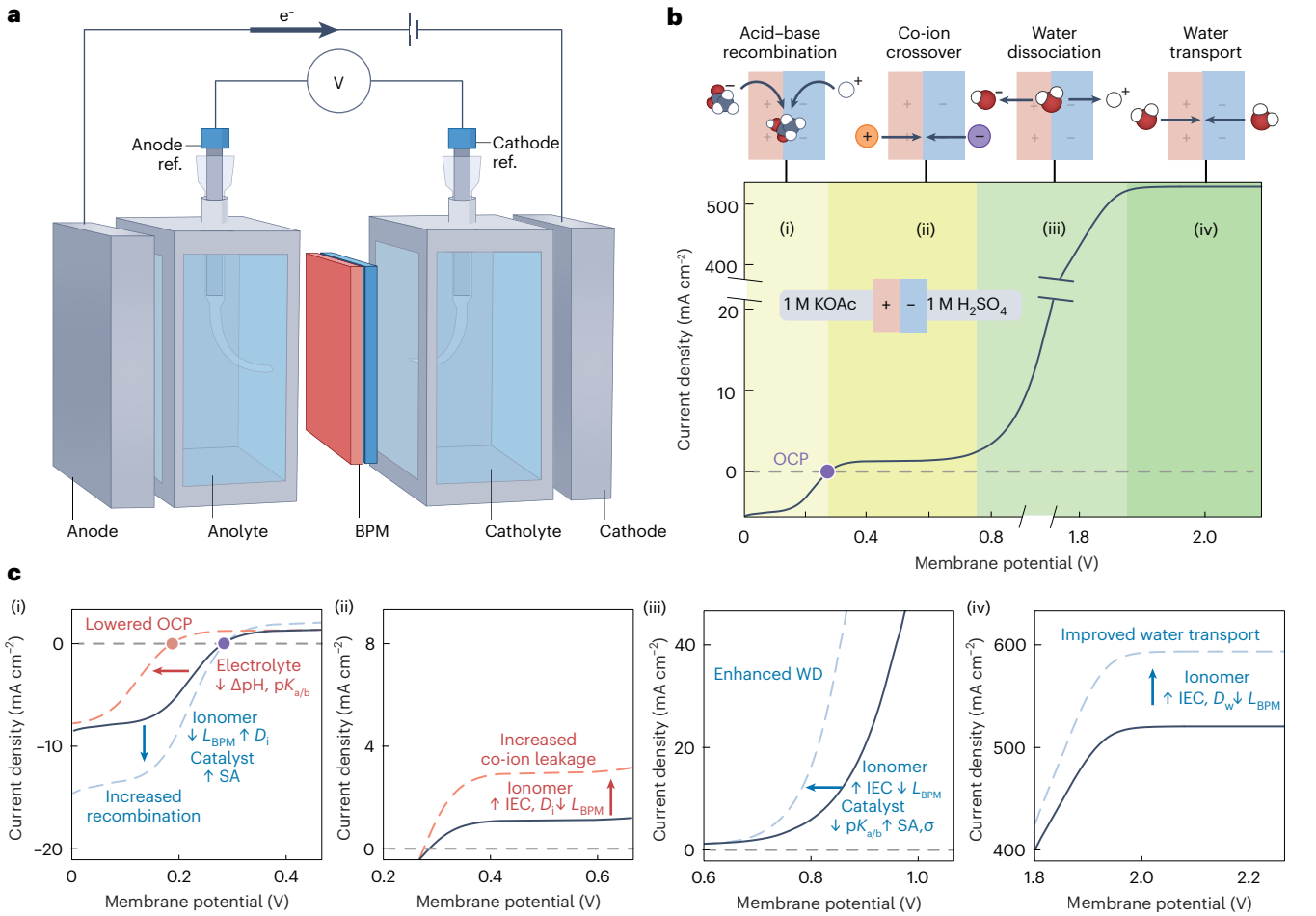

Fig. 3 | Experimental system for characterizing BPMs. a, Schematic of a four-electrode electroanalytical cell, with two reference (ref.) electrodes for operando potential sensing. **b**, Example BPM polarization data broken up into four dominant regimes. **c**, Schematic sensitivity analysis of current–voltage behavior in the (i) acid–base recombination, (ii) co-ion leakage, (iii) WD, and (iv) water-transport regimes to electrolyte (pH, $pK_{a/b}$, ionic diffusivity (D_i)), catalyst (catalyst surface area (SA), electrical conductivity (σ)), and ionomer (BPM thickness (L_{BPM}), water diffusivity (D_w), IEC) properties. The OCP is the applied membrane potential where the current through the BPM is zero.

Structure–property–performance relationships

Advancing BPM development requires understanding of the relationships between structure, physical and transport properties, and performance. BPMs must be capable of achieving high rates of WD or ion recombination, (for energy conversion devices typically ~0.5 to 2 A cm^{-2}) and therefore must be able to facilitate transport of desired species efficiently, while reducing that of undesired species in these often multicomponent systems.

Decreasing the AEL or CEL thickness improves ion and solvent transport by decreasing the transport distance[14,23], which has both beneficial and detrimental (for example, co-ion leakage) aspects depending on the ion. Increasing IEC of the AEL or CEL improves ionic conductivity, but also promotes co-ion leakage due to the enhanced solvent uptake and reduced permselectivity (Fig. 4a). Increasing IEC also compromises mechanical integrity. These trade-offs between throughput and selectivity are well known in the membrane-separation literature[55,58], but have not been understood fully in the context of BPMs, where most work has focused on maximizing throughput (total current density at a given potential) or WD energy efficiency (voltage at a given current density).

Examining trends in reported BPM performance for 53 different BPMs reveals that BPM performance has improved substantially over the last decade. On average, the applied potential to achieve a current density of 100 mA cm^{-2} has dropped significantly (Fig. 4b)[14,57,59]. At the same time, the co-ion leakage observed in these systems has increased by nearly an order of magnitude (Fig. 4c), exhibiting the selectivity and throughput trade-off (Fig. 4e,f). This trade-off can be partially explained by increased IEC and reduced thickness in newer BPMs (Fig. 4e,f). Importantly, many of these demonstrations utilized poor WD catalysts, for which the ohmic and mass-transport losses through the membrane are negligible compared with the WD losses. New high-performance WD catalysis with negligible kinetic loss[13,14,51] enable better optimization of the underlying conductivity–selectivity trade-off.

The persistent balance between throughput and selectivity suggests the need for a paradigm shift in the structural and morphological design of ionomers. For example, performance could be enhanced through the use of ionomers with high fixed-charge density to improve Donnan exclusion and ionic conductivity[21,60]. In such polymers, the impact of confinement and mechanical forces becomes more relevant, as the osmotic and chain-coiling forces will need to be managed to lessen swelling as charge density increases. Improved mechanical stability will also be crucial in enhancing the AEL/CEL interface dimensional stability under the stressors of larger gradients, disparate AEL and CEL properties, and interfacial reactions (for example, CO_2 gas formation). Therefore, managing polymer mechanics (like covalent cross-linking[61]) will be necessary for future applications[60]. Lastly, unique to BPMs is the ability to leverage ion-correlated motion between co-ions and WD-generated H^+/OH^- at high current densities (>200 mA cm^{-2}) to attenuate crossover[14,44]. Hence, leveraging transport properties and

https://doi.org/10.1038/s44286-023-00009-x

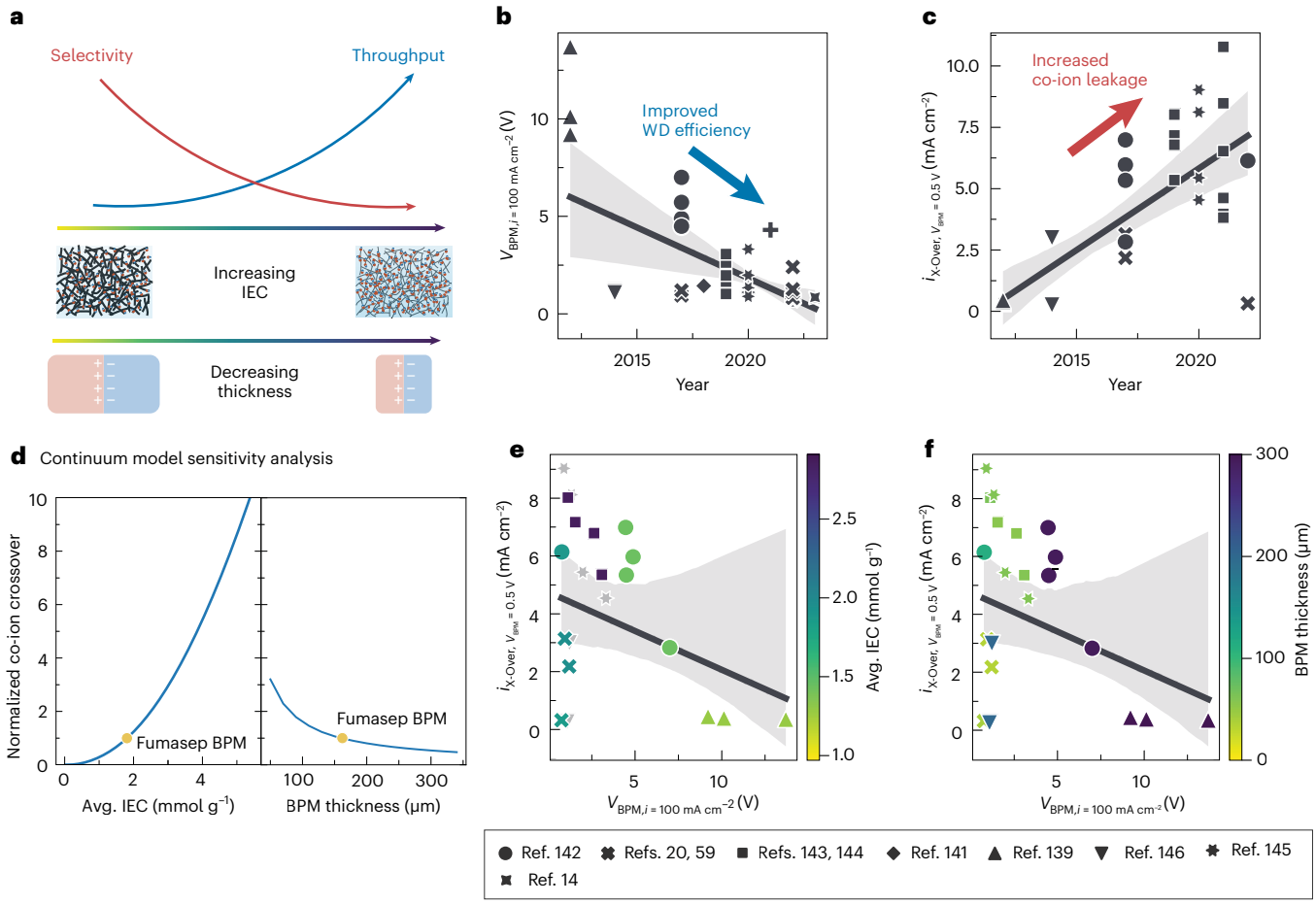

Fig. 4 | Performance trade-offs in BPMs. a, Throughput versus selectivity. **b**, Transmembrane potential required to achieve 100 mA cm^{-2} current density. **c**, Co-ion leakage (measured as current at 0.5 V of transmembrane potential) as a function of publication year for 53 BPMs in literature as measured in four-probe cells. **d**, Simulated sensitivity of co-ion crossover to the average IEC of the BPM and its overall BPM thickness, normalized to the simulated co-ion crossover of the Fumasep BPM[21]. **e**,**f**, Transmembrane potential required to achieve 100 mA cm^{-2} current density versus co-ion leakage for literature BPMs demonstrating the throughput versus selectivity trade-off, with data color-coded by average IEC (**e**) and overall BPM thickness (**f**). BPM performance data are extracted from literature reports[14,20,59,139–146]. Light gray bands in **b**, **c**, **e** and **f** represent a 95% confidence interval in the linear regression.

frictional interactions of ions themselves could facilitate an alternative route to break the throughput/selectivity trade-off.

Applications of BPMs

Water electrolysis and CO_2 reduction

Monopolar anion exchange membrane (AEM) and CEM CO_2 and water electrolyzers require either use of expensive catalysts (for example, IrO_2 at the anode) for acidic CEM systems or poor-performing cathode catalysts and issues with bicarbonate formation and crossover in AEM cells. BPMs in reverse bias could ameliorate the concerns by ensuring low (bi)carbonate crossover and more facile hydrogen-evolution reaction (HER) at the acidic cathode compared to alkaline conditions when using Pt (ref. 62), while enabling inexpensive catalysts for oxygen-evolution reaction (OER) in the alkaline environment, where Fe-, Ni-, and Co-based electrocatalysts have demonstrated operation at 1 A cm^{-2} at total cell potentials between 1.65–2.15 V in water electrolyzers, commensurate with that of IrO_2 in acidic ones (Fig. 5a)[63–67].

Physically, there is no reason that BPM water electrolyzers cannot operate with the same or better efficiency than AEM or proton-exchange membrane (PEM) water electrolyzers, with literature showing near parity with AEM water electrolyzers[57] (Fig. 5b), with optimized WD overpotentials of less than 50 mV at 20 mA cm^{-2} (refs. 13,14,20,57,59). Whereas the BPM performs WD at the AEL/CEL interface, AEM or CEM water electrolyzers also perform WD, perhaps as a step in the electrocatalytic mechanism, at the electrode surface to facilitate alkaline HER or acidic OER, respectively. Because the thermodynamics of the reaction chemistry in these three systems are identical, the differences in cell-level performance must be attributed to non-equilibrium energy losses—in particular, the kinetic losses at the electrocatalysts and the WD catalyst. In BPM water electrolyzers, the kinetic overpotential associated with WD remains a significant energy loss[13].

Due to CO_2 solubility and acid/base chemistry, CO_2 electrolyzers typically operate under alkaline conditions, although acidic ones would still require expensive catalysts[68]. If AEMs are used, the transport of (bi)carbonates formed from the CO_2 reagent and anionic CO_2 reduction products such as acetate and formate from cathode to anode is problematic[69]. This characteristic of AEMs increases the CO_2 electrolyzer capital cost, which hinders scalability. BPMs address this challenge by transporting H^+ to the cathode to neutralize (bi)carbonates before they cross over[70–72]. The Donnan exclusion of (bi)carbonates from the CEL further limits (bi)carbonate crossover (Fig. 5c,d). BPMs can also modulate the local environment at the cathode to promote CO_2R to methane and other C_1 products with copper catalysts[73]. Moreover, BPMs mitigate the crossover of neutral CO_2R products through frictional interactions with WD-generated H^+/OH^- (ref. 74), which is particularly important when producing solution-phase products.

A challenge with using reverse-bias BPMs in CO_2 electrolyzers, however, is demonstrated stability and scalability, and over-acidification

https://doi.org/10.1038/s44286-023-00009-x

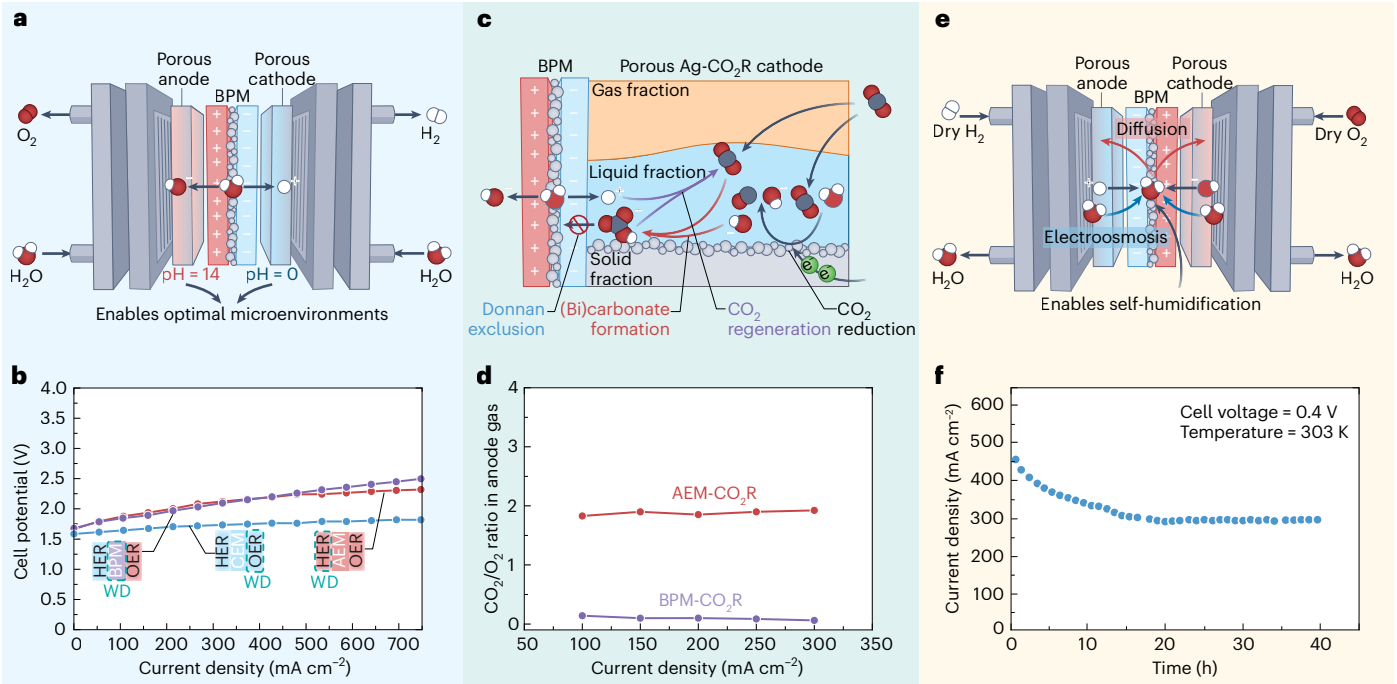

Fig. 5 | MEAs using BPMs. a–**f**, MEAs for water electrolysis (**a**,**b**), CO_2R (**c**,**d**), and hydrogen fuel cells (**e**,**f**). **a**, Schematic of a BPM electrode assembly for water electrolysis. **b**, Comparison of performance for an AEM, CEM, and BPM water electrolyzer[66]. **c**, Schematic of CO_2 regeneration in a BPM. **d**, Comparison of CO_2 crossover in an AEM and BPM CO_2R device[92]. **e**, Schematic of a self-humidifying hydrogen fuel cell employing a BPM. **f**, BPMs facilitate improved stability and lifetime when operating with dry H_2 and O_2 feeds[93]. Panels adapted with permission from: **b**, ref. 23, American Chemical Society; **d**, ref. 76 under a Creative Commons license CC BY 4.0; **f**, ref. 94, Elsevier.

of the cathode, which leads to high rates of HER over CO_2R. Aqueous and solid-state buffer layers placed in between the cathode and CEL can increase the residence time for H^+ to neutralize (bi)carbonates produced near the cathode[75,76]. Similarly, using a weakly acidic CEL (a low IEC) can improve selectivity for CO_2R over HER by attenuating the H^+ flux to the cathode[77]. However, the use of a buffer layer or lower IEC CEL ultimately increases the electrolyzer ohmic losses, a trade-off that must be considered in device design.

CO_2R electrolyzers with BPMs have also been used to reduce concentrated (bi)carbonate solutions, as opposed to CO_2 gas, into CO[78–82], formate[83], and methane[73]. The outward flux of H^+ from the CEL of the BPM drives conversion of (bi)carbonates into CO_2 locally, which is then reduced at a porous electrode. The benefit of BPM (bi)carbonate electrolysis is that it bypasses the need to isolate CO_2 upstream of the electrolyzer, could overcome low CO_2 solubility, and produces CO_2R products with minimized unreacted CO_2 in the product streams. However, commercial BPMs used in bicarbonate electrolyzers to date have required high voltages[84]. BPMs with faster WD catalysts are anticipated to improve (bi)carbonate electrolyzer performance.

Forward bias BPMs for energy storage and conversion

Using a forward-biased BPM, the chemical potential stored in separated acid and base can be recovered as electrical work, and have been shown to enable aqueous redox-flow batteries (RFBs) with cell voltages >2 V (above the conventional water-stability window of 1.23 V), thus possibly providing higher energy and power densities[85–87]. This is because while the electrodes drive Faradaic reactions, the BPM generates or consumes the acid and base[87–90]. For example, the overall cell reaction for a BPM RFB could be

$$O_1^{\text{anolyte}} + R_2^{\text{catholyte}} + H_2O \leftrightarrow R_1^{\text{anolyte}} + O_2^{\text{catholyte}} + H^{+,\text{anolyte}} + OH^{-,\text{catholyte}} \quad (9)$$

where two redox couples O_1/R_1 and O_2/R_2 differ in charge state by one.

BPM acid–base RFBs enable energy storage in the chemical potential gradient across the BPM. However, energy losses in these systems resulting from co-ion transport and ohmic losses ranged from 39–65%, significantly more than what is acceptable for scale up[91]. New BPMs, therefore, must be engineered with high permselectivities in highly concentrated electrolytes.

Forward-bias BPMs can also be used in BPM fuel cells (BPMFCs), which feature acidic anodes and alkaline cathodes. These dissimilar local pHs allow the hydrogen-oxidation reaction and oxygen-reduction reaction (ORR) to operate both with facile kinetics and inexpensive non-platinum ORR catalysts[92,93]. BPMFCs are also self-humidifying, where the electrodes are hydrated via the outward diffusion of H_2O that accumulates in the junction and is generated during operation[94]. A BPMFC under dry-gas conditions (Fig. 5e,f), achieved a power density of 327 mW·cm^{-2} at 323 K and observed self-humification with in situ attenuated total reflectance-Fourier transform infrared spectroscopy (ATR-FTIR)[94]. In these systems, modeling has shown that the self-humidification effect can be enhanced by improving AEL water transport and reducing its thickness[95].

When ionic species combine at the AEL/CEL interface in a forward-bias BPM, the OCP scales according to the $pK_{a/b}$ of the produced acid or base (that is, $V_{mem} = 59$ mV·$pK_{a/b}$), as opposed to the transmembrane pH gradient as expected by Nernst equilibria[21,35]. It has been demonstrated that the dependence of the OCP on the $pK_{a/b}$ is due to co-ion crossover and interfacial buffering (denoted as 'neutralization short-circuiting'; Fig. 6)[35]. Neutralization short-circuiting occurs when OH^- or H^+ reacts with weak acid (AH^+; $pK_a > 0$) or base (B^-; $pK_a < 14$) thus consuming some of the chemical potential and reducing the OCP by lowering the $pK_{a/b}$ of the produced conjugate acid/base (A and BH) compared with water.

Aside from reducing the OCP, the presence of competing counter-ions also induces limiting-current densities in forward bias. Consider the asymmetric KOH/OAc|H_2SO_4 system (Fig. 6d)[96]. At low forward-bias current densities, H^+/OH^- recombination in the junction dominates because of the fast reaction kinetics (kinetic control). However, the

https://doi.org/10.1038/s44286-023-00009-x

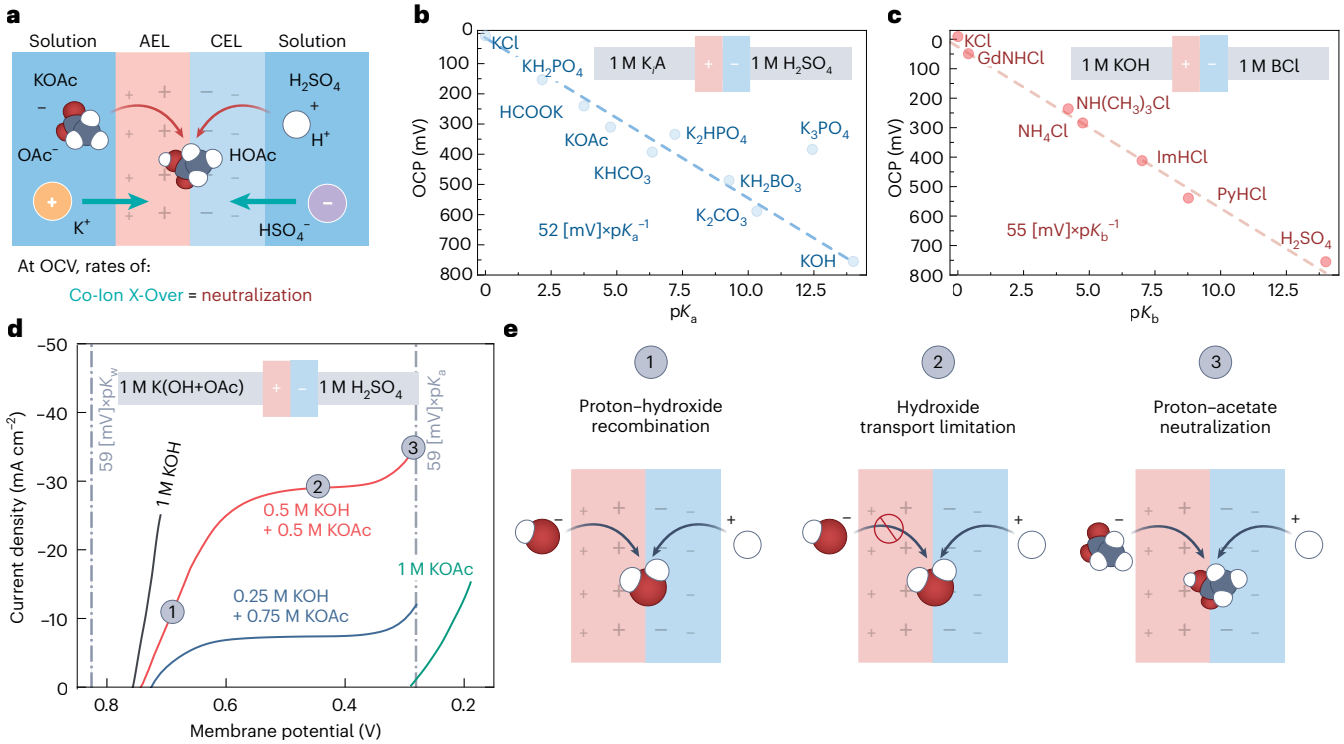

Fig. 6 | Acid–base recombination effects for BPMs operating in forward bias. **a**, Schematic of neutralization short circuiting in BPMs. **b**,**c**, Impact of pK_a (**b**) and pK_b (**c**) of weak-buffer electrolytes on OCP[35]. **d**, Impact of electrolyte impurities on current-density performance in forward bias[96]. **e**, Schematic mechanisms for regimes of the forward-bias polarization under acid–base recombination conditions. Panels adapted with permission from: **b**,**c**, ref. 35, American Chemical Society; **d**, ref. 96, Springer Nature Ltd.

transport of OH^- eventually becomes limiting due to interfacial buffering and competition with OAc^- for fixed cation sites in the AEL, creating a voltage-independent current plateau (transport control). The plateau in current ends when the voltage required to protonate OAc^- is reached, and the recombination of H^+ with OAc^- then dictates the current density. Notably, this current plateau resulting from a combination of transport limitations and ion-selective partitioning helps explains the low limiting-current densities observed in most demonstrations of forward-bias BPMs for RFBs, where redox-active counter-ions compete with H^+/OH^- and attenuate the current density. Therefore, the effects of selective (non-ideal) ion-partitioning in concentrated solutions must be considered to understand ion speciation and manage neutralization short-circuiting in forward-bias BPMs.

Acid–base generation for environmental remediation

Acid–base production is key to driving chemistries that capture and mineralize CO_2, de-acidify ocean waters, upcycle nitrogenous wastewater contaminants to ammonia, and produce clean cement via the conversion of $CaCO_3$ into $Ca(OH)_2$ (Fig. 7). Each of these processes relies on a continuous supply of acid and base to modulate the buffer equilibria of inorganic carbon and nitrogen species. However, the most widely produced acids and bases in industry, H_2SO_4 and NaOH, are formed as by-products of natural-gas desulfurization and chlorine-gas manufacturing, respectively. The large-scale production of acid and base can be accomplished by electrolysis or electro-deionization processes, where the HER and OER produce H^+ and OH^-, respectively. However, the need to concurrently produce H_2 and O_2 with acid and base increases electricity consumption because of the high overpotentials associated with OER.

Because BPMs can dissociate water into H^+ and OH^- without gas generation, the thermodynamic and kinetic losses associated with H_2 and O_2 formation in electrolytic acid–base production are eliminated. This feature enables many BPM cells to be operated in series with only two terminal electrodes (thereby reducing overall capital cost and increasing energy density) in a process known as electrodialysis (ED). As a result, BPM-ED has a lower theoretical energy consumption of 0.83 V (80 kJ mol^{-1}) when producing products at their standard state compared with 1.23 V (237 kJ mol^{-1}) for electrolysis/electro-deionization processes that must also have a mole of H_2 and half a mole of O_2 for every mole of acid and base. Each BPM in a BPM-ED stack can be paired with combinations of AEMs and/or CEMs, and the resulting unit (BPM-CEM, BPM-AEM, BPM-AEM-CEM, and so on) comprises the repeating unit for the ED process (Fig. 7)[30].

CO_2 removal from seawater is another emerging application of BPM-ED. The H^+ produced by WD is used to convert dissolved (bi) carbonates naturally present in seawater (~0.02 mM) into CO_2 for sequestration or conversion, and the OH^- is circulated back to the ocean to promote atmospheric drawdown of CO_2 (Fig. 7a). The OH^- from the BPM can also be used to produce mineralized carbonate species synthetically[8,97]. Correspondingly, BPM-ED can capture CO_2 and re-generate sorbents in direct-air-capture schemes (Fig. 7b)[30,98,99]. Although the majority of BPMs used for direct air capture are operated in reverse-bias, it has been demonstrated that a forward-bias BPM can also accelerate CO_2 capture. Key to this system is the use of a microporous, interfacial solid-electrolyte layer composed of styrene-divinylbenzene copolymers functionalized with sulfonate groups. Within this micro-structured interface, sulfonate groups facilitate H^+ transport and the microporosity provides transport pathways for (bi)carbonates to recombine with H^+ to form pure CO_2 and water[100].

Another application of BPM-ED involves the conversion of limestone into cement clinker precursor, addressing a need to reduce the emissions from thermal calcination ($CaCO_3$ + heat → CaO + CO_2) in cement manufacturing[101,102]. H^+ from the BPM is used to acidify $CaCO_3$ to form CO_2 and Ca^{2+}, which is then transported across a CEM where it combines with OH^- from an adjacent BPM to form $Ca(OH)_2$.

https://doi.org/10.1038/s44286-023-00009-x

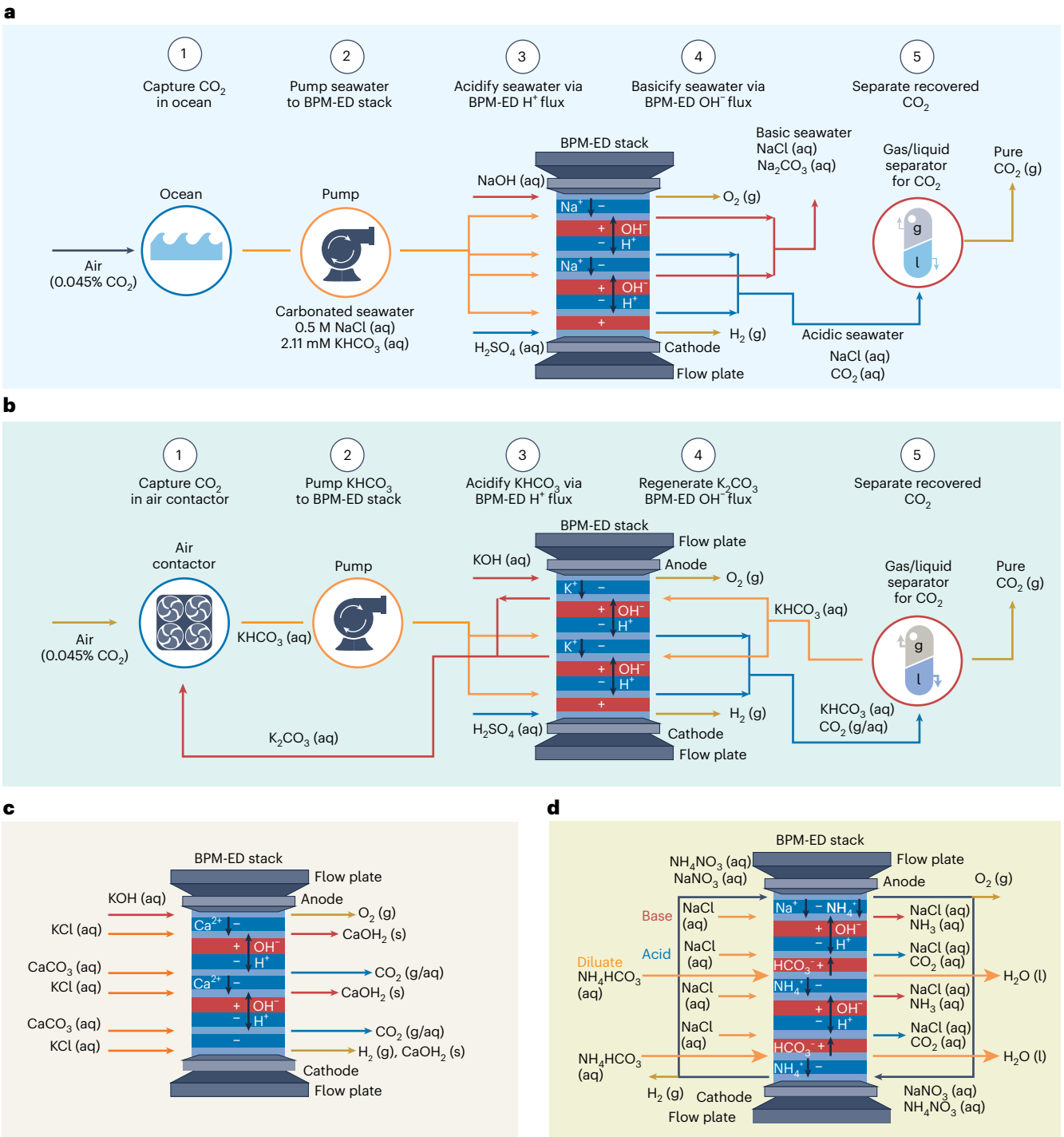

Fig. 7 | Process schematics for BPM-ED systems applied in environmental remediation processes. a, Direct ocean capture. **b**, Direct air capture. **c**, Cement clinker precursor production. **d**, Ammonia recovery via BPM-ED. Red indicates alkaline streams or AEMs; blue indicates acidic streams or CEMs; orange indicates neutral or near-neutral streams; yellow indicates gaseous streams.

The $Ca(OH)_2$ is then converted directly to CaO as a drop-in cement additive (Fig. 7c)[101].

Ammonia is an industrial chemical produced by chemical reduction of N_2 with H_2, produced by steam methane reforming, and its use in fertilizers is responsible for the high levels of nitrogenous waste (particularly ammonium and nitrate ions) found in lakes and rivers[103]. BPM-ED can address these issues using the pH-dependent equilibrium between dissolved ammonium found in wastewater and ammonia for fertilizer production. BPM-ED has been used to produce ammonia from ammonium at an energy intensity of 266 kJ per mol of NH_3 (ref. 104). They also used the BPM-ED process to desalinate simultaneously the wastewater thereby producing a pure-water stream (Fig. 7d). BPM-ED can also recover ammonia from urine. In this system, an ion-exchange resin positioned on the cathode side of the BPM is used to first capture urine that is then acidified to produce ammonia[105]. For these applications, BPM materials must be improved to reduce chemical incompatibility with dissolved nitrogen species and mitigate crossover of the produced NH_4^+; the use of a thick AEL can help mitigate this crossover.

https://doi.org/10.1038/s44286-023-00009-x

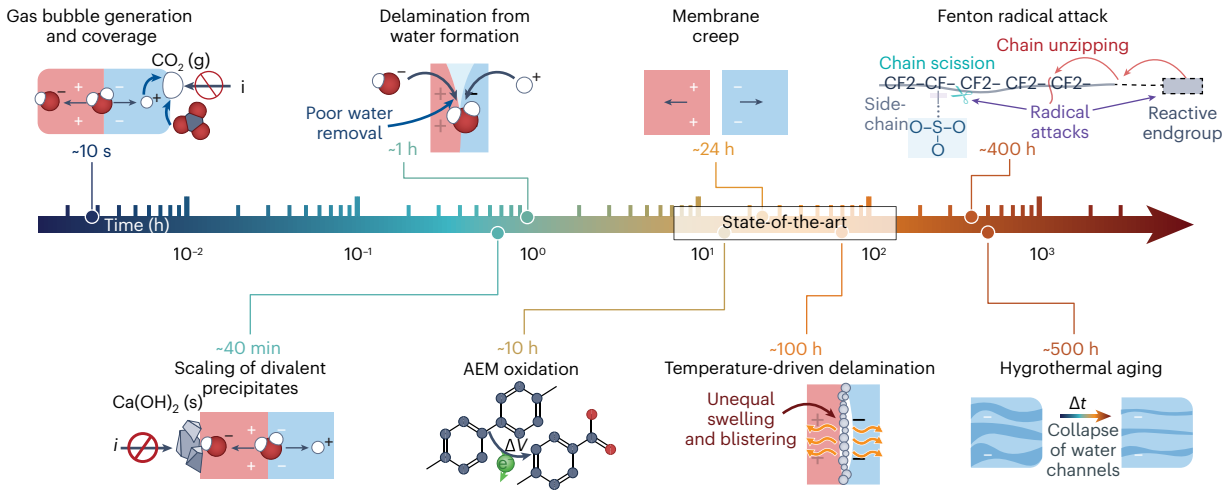

Fig. 8 | Timeline of physical and chemical BPM degradation modes. These processes occur over different timescales in BPMs. Timescale of failure for state-of-the-art BPMs are highlighted in the box.

One of the major challenges with BPM-ED is ion fouling and low energy efficiency[101]. This nascent technology will need to make significant headway in terms of stability, efficiency, and scale to be commercially relevant. Additionally, ion transport limitations of the individual monopolar membranes, as the individual ion-exchange polymers are not conductive for transporting ions other than H^+/OH^-. Hence, these systems will not only require fast WD kinetics, but also high permselectivity for H^+ and OH^- to mitigate crossover of impurities present in high concentrations in the feed streams and improve transport[102]. A primary challenge of BPM-ED is the high capital cost and operating costs[106], which must be addressed through device engineering and the development of new BPMs. Learnings from traditional membrane processes (for example, anti-fouling techniques[107] and pretreatment[108]) and unit operations concepts can be leveraged to optimize practical cell and stack designs.

Challenges for BPM applications

Management of impurities in real process streams

The distinct capabilities of BPMs to enforce ion management makes them attractive candidate materials for use with impure water streams like seawater, tap water, and lakes. Management of such ions poses significant challenges to electrolyzer energy efficiency, selectivity, and durability. Recent developments in BPMs have demonstrated progress towards direct electrolysis of impure water and seawater, holding promise for the generation and distribution of delocalized H_2 from offshore and coastal sites, as well as the use of BPM electrolysis to generate O_2 for life support in underwater applications[109].

The challenge of divalent contaminant scaling via inorganic precipitation is particularly damaging for systems that manage substantial amounts of Ca^{2+} or Mg^{2+}. For instance, a key challenge in cement-clinker-precursor production using BPM-ED (Fig. 7c) is the scaling of $Ca(OH)_2$(s) due to reaction of WD-generated OH^- with Ca^{2+} from the CEMs that appear between repeat BPM units. This issue has been avoided by employing thin polyaniline layers over the CEMs to exclude Ca^{2+} cations via Donnan exclusion, and enable these cations to be transported out of the cell by convection[102]. A supporting KCl electrolyte is co-fed, and the K^+ becomes the charge carrier in the repeat CEMs. Mixing of Ca^{2+} with electrochemically generated OH^- occurs outside of the cell to produce $Ca(OH)_2$(s) and allows for at least 50 h of stable operation at 100 mA cm^{-2} (ref. 103). Other strategies in improving BPM resilience towards inorganic precipitation include modifying the electrode porosity, introducing open areas not in direct contact with the electrode, and recovery procedures such as pulsing electric-field polarity and feed acidification[110–113].

Chloride (Cl^-) ions are challenging impurities for electrochemical devices, for example, impure water electrolysis, as their oxidation to corrosive chlorine species (Cl_2, HOCl, OCl^-) is more kinetically facile than OER, despite being less favorable thermodynamically[114,115]. BPM electrolyzers have leveraged reactor designs to mitigate the formation of such chlorine species[115] via AEL and CEL permselectivity. At low current densities (50 mA cm^{-2}), a CEL in a BPM can minimize transmembrane Cl^- crossover to less than 2% of the total ionic charge, decreasing to 0.1% at high current densities (500 mA cm^{-2})[44]. The non-intuitive, current-density-dependent co-ion crossover indicates that concentrated-solution theories are necessary to understand the trends. Ion-correlated movement between generated H^+/OH^- and co-ions could explain the reduced co-ion crossover at high current densities, wherein H^+ and OH^- efflux out of the membrane slows the movement of co-ion influx. Analogously, cation crossover is inhibited by the BPM AEL. Ion crossover in BPMs is further a function of ion/molecule size and ion valence, offering additional tools to control ion transport by appropriate AEL and CEL design[116]. Feeding impure water to the cathode and pure water to the anode is an operational strategy that reduces the local anode Cl^- concentration by blocking anion transport and preferentially forming O_2 over chlorine species because the basic anode microenvironment promotes water over chlorine oxidation[111,117]. The efficacy of such BPM operation has been shown to extend device lifetime to >100 h using base[110,111], water vapor[118], or pure water[44] as the anode feed.

Finally, in real process streams such as seawater, trace amounts of organic matter are often present. The uptake of non-polar organic species in ionomers leads to reduced ionic conductivity due to mixing of the organics with polymer side chains, which disrupts ionomer morphology[119]. Management of the organics, perhaps through decomposition at the anode, and a fundamental understanding of solvent partitioning are required for applications with such process streams.

Material durability and reactor stability

While recent advances in BPM performance suggest their integration into scalable reactors will soon be realized, stability and durability are tantamount and remain challenges as noted in recent techno-economic analyses[16,101,106]. BPMs need to last on the order of years, not the currently demonstrated hundreds of hours[106], to be on par with those demonstrated for traditional membrane-based processes[120]. To arrive at these milestones, degradation phenomena and failure modes need to be elucidated and ameliorated across multiple timescales (Fig. 8). Furthermore, most studies focus on relatively low current densities (<50 mA cm^{-2}) and not under the more demanding and industrially

relevant high fluxes (>1 A cm^{-2}), where transport, heat, and mechanical effects combine to enhance failure stressors as described below.

Freestanding BPMs (those which possess sufficient AEL/CEL adhesion such that they do not need to be mechanically supported) are important for ease of cell design, size, and integration. Commercial BPMs (for example, from Neosepta or Fumasep), are mechanically robust with AEL and CEL well-adhered to each other and incorporated into a reinforced mesh[1]. Newer research-level BPMs possess substantially improved voltage performance, but do not appear to have reached this level of mechanical durability. Laminated CELs and AELs typically have strong adhesion due to electrostatic interactions between the oppositely-charged ionomers[121]. Integration of a CL, however, typically reduces the mechanical adhesion[1,14]. Insufficient mechanical adhesion results in membrane blistering and even delamination, particularly in forward-bias where water accumulation stresses the interface[2], which requires interface engineering and can benefit from traditional chemical-engineering insights and approaches. Water management is also crucial in reverse bias. Irreversible damage has been observed of a Fumasep-FBM operated in reverse bias at current densities exceeding 600 mA cm^{-2} due to water-transport limitations and dryout of the interface[59], which is exacerbated by a mismatch in ionomer transport properties (for example, electroosmotic coefficients) at high fluxes. One strategy for increasing mechanical integrity of BPMs is to electrospin interpenetrating nanofibers into the bipolar junction[20,59,122]. Solid formation of scaling precipitates is also key to consider in BPM durability[113].

Recently, a freestanding graphene-oxide-catalyzed BPM with intrinsic interfacial adhesion has been reported, attributed to favorable electrostatic interactions facilitated by the graphene-oxide layer that was mixed with Nafion dispersion[14]. The BPM exhibited stable performance >100 h at 500 mA cm^{-2}, wherein failure was attributed due to temperature-driven delamination of the AEL and CEL. Understanding and quantifying the mechanism of adhesion and subsequent delamination of the AEL, CEL, and CLs is needed to develop BPM integration design rules and mitigation methods (for example, use of porous separators) for mechanically robust catalyzed BPMs.

BPMs operated in a zero-gap assembly require stability at the electrode/BPM interfaces. To date, this stability has not been directly assessed; however, the instability of AEMs under oxidative conditions has been identified as a failure mode in both AEM water electrolyzers and fuel cells[65,123–125]. Previous work has observed the oxidation of ionomer phenyl groups to phenol when contacting the catalyst surface under alkaline OER conditions[123], and X-ray photoelectron spectroscopy (XPS) analysis indicates degradation and dissolution of the piperidinium solvating unit[124,126]. Similarly, ionomer oxidation has been shown at ORR potentials in AEM fuel cells[127]. Oxidative stability of the AEL must be realized for sustainable zero-gap operation, thus engineering oxidatively stable AELs should be prioritized. Interface engineering of the electrocatalysts may enhance stability by controlling deleterious ions, perhaps via passivated catalysts that mitigate charge transfer between the ionomer and catalyst or alternatively by integrating artificial solid-electrolyte-interphases, which is common in the battery community.

Once short-time scale stressors have been managed, long-term chemical and mechanical degradation, must be addressed[128,129]. The primary chemical degradation mechanism in PFSA ionomers results from hydroxyl radical formation from peroxide degradation (a result of H_2/O_2 crossover and ORR), which initiate chain scission and unzipping, thus degrading the membranes[18,130,131]. Radical scavengers such as Ce and Mg ions quench formed radicals before radical-driven decomposition[132–134]. At longer time scales, hygrothermal chemical/mechanical aging impact ionomer properties[135]. Membrane creep, in particular, is known to cause electrical shorts and gas crossover through ionomer layers over time due to the compressive stress in electrolyzers[136,137]. Understanding how mechanical stressors effect chemical stressors, and vice versa, will be critical to designing and integrating stable BPMs.

Future perspectives

BPMs can independently and selectively control ion concentrations (for example, pH) and fluxes, making them useful for application within a broad array of electrochemical systems, including those for reactive separations, electrocatalysis, and energy conversion. Recent advances in WD catalysis and interface engineering have improved BPM performance dramatically, decreasing the voltage at 1 A cm^{-2} by >1 V. These advances along with general electrification have enabled new BPM applications, such as in electrolysis, fuel cells, and carbon capture—all areas where throughput and energy efficiency are critical. To accelerate device development, however, many aspects of BPMs should be further improved, and engineering approaches guided by multi-scale physics will be essential in this effort. For example, coupled thermodynamics and transport phenomena embedded in concentrated-solution theories are necessary to model and understand ion-correlated motion and mechanisms of ion crossover and water transport. Similarly, one needs to examine the coupled behavior of the underlying phenomena and governing design rules when scaling up and integrating assemblies. Asymmetric BPMs with varying material properties could leverage the emergent properties of the BPM composite to facilitate greater functionality, but also may reveal new failure modes that must be understood. For example, understanding the connection between ionomer and interface chemistry and mechanical properties is central to developing and integrating novel BPMs in architectures that are durable, as well as in the development of accelerated-stress tests. Other science areas include the mechanistic understanding of WD and H^+/OH^- recombination on catalysts, particularly metal-oxide nanoparticles, where there are diverse sites where protons can absorb and modulate the local electric-field intensity by different degrees of screening. Experimental approaches to map electric fields and pH gradients at equilibrium and during operation would be useful. In addition, new ion-conducting polymers with higher fixed-charge densities and with controlled size sieving could be used to uncouple selectivity and conductivity, with a focus on (safe) fluorine-free ionomers that do not release harmful degradation products and contaminants. Finally, techno-economic analyses are critical for determining key performance indicators (transmembrane voltage loss, ion selectivity, and lifetime) and their relative importance.

References

1. Blommaert, M. A. et al. Insights and challenges for applying bipolar membranes in advanced electrochemical energy systems. *ACS Energy Lett.* **6**, 2539–2548 (2021).
2. Pärnamäe, R. et al. Bipolar membranes: a review on principles, latest developments, and applications. *J. Memb. Sci.* **617**, 118538 (2021).
3. Bui, J. C. et al. Continuum modeling of porous electrodes for electrochemical synthesis. *Chem. Rev.* **122**, 11022–11084 (2022).
4. Mafé, S. & Ramirez, P. Electrochemical characterization of polymer ion-exchange bipolar membranes. *Acta Polym.* **48**, 234–250 (1997).
5. Mafé, S., Ramírez, P. & Alcaraz, A. Electric field-assisted proton transfer and water dissociation at the junction of a fixed-charge bipolar membrane. *Chem. Phys. Lett.* **294**, 406–412 (1998).
6. Craig, N. P. *Electrochemical Behavior of Bipolar Membranes*. PhD thesis, Univ. California, Berkeley (2013).
7. Bui, J. C. et al. Engineering catalyst – electrolyte microenvironments to optimize the activity and selectivity for the electrochemical reduction of CO_2 on Cu and Ag. *Acc. Chem. Res.* **55**, 484–494 (2022).
8. Sharifian, R., Wagterveld, R. M., Digdaya, I. A., Xiang, C. & Vermaas, D. A. Electrochemical carbon dioxide capture to close the carbon cycle. *Energy Environ. Sci.* **14**, 781–814 (2021).

9. Frilette, V. J. Preparation and characterization of bipolar ion-exchange membranes. *J. Phys. Chem.* **60**, 435–439 (1956).
10. Bazinet, L., Lamarche, F. & Ippersiel, D. Bipolar-membrane electrodialysis: applications of electrodialysis in the food industry. *Trends Food Sci. Technol.* **9**, 107–113 (1998).
11. Wilhelm, F. G. *Bipolar Membrane Electrodialysis: Membrane Development and Transport Characteristics*. PhD thesis, Univ. Twente (2001).
12. Garcia-Herrero, I., Margallo, M., Onandía, R., Aldaco, R. & Irabien, A. Connecting wastes to resources for clean technologies in the chlor-alkali industry: a life cycle approach. *Clean Technol. Environ. Policy* **20**, 229–242 (2018).
13. Chen, L., Xu, Q. & Boettcher, S. W. Kinetics and mechanism of heterogeneous voltage-driven water-dissociation catalysis. *Joule* https://doi.org/10.1016/j.joule.2023.06.011 (2023).
14. Lucas, É. et al. Asymmetric bipolar membrane for high current density electrodialysis operation with exceptional stability. Preprint at *ChemRxiv* https://doi.org/10.26434/chemrxiv-2023-n4c6x (2023).
15. Mitchell, J. B., Chen, L., Langworthy, K., Fabrizio, K. & Boettcher, S. W. Catalytic proton-hydroxide recombination for forward-bias bipolar membranes. *ACS Energy Lett.* **7**, 3967–3973 (2022).
16. Ankoliya, D. et al. Techno-economic analysis of integrated bipolar membrane electrodialysis and batch reverse osmosis for water and chemical recovery from dairy wastewater. *J. Clean. Prod.* **420**, 138264 (2023).
17. Boettcher, S. et al. Water-dissociation catalysis near the reversible limit in bipolar membrane electrolyzers. Preprint at *Research Square* https://doi.org/10.21203/rs.3.rs-3447094/v1 (2023).
18. Kusoglu, A. & Weber, A. Z. New insights into perfluorinated sulfonic-acid ionomers. *Chem. Rev.* **117**, 987–1104 (2017).
19. Zhang, K., Yu, W. S., Ge, X., Wu, L. & Xu, T. Molecular dynamics insight into phase separation and transport in anion-exchange membranes: effect of hydrophobicity of backbones. *J. Memb. Sci.* **661**, 120922 (2022).
20. Powers, D. et al. Freestanding bipolar membranes with an electrospun junction for high current density water splitting. *ACS Appl. Mater. Interfaces* **14**, 36092–36104 (2022).
21. Bui, J. C., Digdaya, I., Xiang, C., Bell, A. T. & Weber, A. Z. Understanding multi-ion transport mechanisms in bipolar membranes. *ACS Appl. Mater. Interfaces* **12**, 52509–52526 (2020).
22. Luo, X. et al. Anion exchange ionomers: impact of chemistry on thin-film properties. *Adv. Funct. Mater.* **31**, 2008778 (2021).
23. Oener, S. Z., Twight, L. P., Lindquist, G. A. & Boettcher, S. W. Thin cation-exchange layers enable high-current-density bipolar membrane electrolyzers via improved water transport. *ACS Energy Lett.* **6**, 1–8 (2021).
24. Thiele, S. et al. Bipolar membrane electrode assemblies for water electrolysis. *ACS Appl. Energy Mater.* **3**, 9635–9644 (2020).
25. Goyal, P., Kusoglu, A. & Weber, A. Z. Coalescing cation selectivity approaches in ionomers. *ACS Energy Lett.* **8**, 1551–1566 (2023).
26. Crothers, A. R., Darling, R. M., Kusoglu, A., Radke, C. J. & Weber, A. Z. Theory of multicomponent phenomena in cation-exchange membranes: part II. Transport model and validation. *J. Electrochem. Soc.* **167**, 013548 (2020).
27. Kamcev, J. et al. Partitioning of mobile ions between ion exchange polymers and aqueous salt solutions: importance of counter-ion condensation. *Phys. Chem. Chem. Phys.* **18**, 6021–6031 (2016).
28. Crothers, A. R., Darling, R. M., Kusoglu, A., Radke, C. J. & Weber, A. Z. Theory of multicomponent phenomena in cation-exchange membranes: part I. Thermodynamic model and validation. *J. Electrochem. Soc.* **167**, 013547 (2020).
29. Parasuraman, A., Lim, T. M., Menictas, C. & Skyllas-Kazacos, M. Review of material research and development for vanadium redox flow battery applications. *Electrochim. Acta* **101**, 27–40 (2013).
30. Bui, J. C. et al. Analysis of bipolar membranes for electrochemical capture from air and oceanwater. *Energy Environ. Sci.* https://doi.org/10.1039/D3EE01606D (2023).
31. Onsager, L. Deviations from Ohm's law in weak electrolytes. *J. Chem. Phys.* **2**, 599–615 (1934).
32. Mareev, S. A. et al. A comprehensive mathematical model of water splitting in bipolar membranes: Impact of the spatial distribution of fixed charges and catalyst at bipolar junction. *J. Memb. Sci.* **603**, 118010 (2020).
33. Onishi, N., Minagawa, M., Tanioka, A. & Matsumoto, H. Current–voltage characteristics and solvent dissociation of bipolar membranes in organic solvents. *Membranes* **12**, 1236 (2022).
34. Wesley, T. S., Román-Leshkov, Y. & Surendranath, Y. Spontaneous electric fields play a key role in thermochemical catalysis at metal-liquid interfaces. *ACS Cent. Sci.* **7**, 1045–1055 (2021).
35. Dinh, H. Q., Toh, W. L., Chu, A. T. & Surendranath, Y. Neutralization short-circuiting with weak electrolytes erodes the efficiency of bipolar membranes. *ACS Appl. Mater. Interfaces* **15**, 4001–4010 (2023).
36. Pärnamäe, R. et al. Origin of limiting and overlimiting currents in bipolar membranes. *Environ. Sci. Technol.* **57**, 9664–9674 (2023).
37. Newman, J. & Thomas-Alyea, K. E. *Electrochemical Systems* (John Wiley and Sons, 2004).
38. Bird, B. R., Stewart, W. E. & Edwin, N. L. *Transport Phenomena*. (Wiley, 2007).
39. Bui, J. C., Corpus, K. R. M., Bell, A. T. & Weber, A. Z. On the nature of field enhanced water dissociation in bipolar membranes. *J. Phys. Chem. C* **125**, 24974–24987 (2021).
40. Peng, J., Roy, A. L., Greenbaum, S. G. & Zawodzinski, T. A. Effect of CO_2 absorption on ion and water mobility in an anion exchange membrane. *J. Power Sources* **380**, 64–75 (2018).
41. Ehlinger, V. M., Crothers, A. R., Kusoglu, A. & Weber, A. Z. Modeling proton-exchange-membrane fuel cell performance/degradation tradeoffs with chemical scavengers. *J. Phys. Energy* **2**, 044006 (2020).
42. Petrov, K. V. et al. Anion-exchange membranes with internal microchannels for water control in CO_2 electrolysis. *Sustain. Energy Fuels* **6**, 5077–5088 (2022).
43. Weng, L. C., Bell, A. T. & Weber, A. Z. A systematic analysis of Cu-based membrane-electrode assemblies for CO_2 reduction through multiphysics simulation. *Energy Environ. Sci.* **13**, 3592–3606 (2020).
44. Marin, D. H. et al. Hydrogen production with seawater-resilient bipolar membrane electrolyzers. *Joule* **7**, 765–781 (2023).
45. Fong, K. D., Bergstrom, H. K., McCloskey, B. D. & Mandadapu, K. K. Transport phenomena in electrolyte solutions: nonequilibrium thermodynamics and statistical mechanics. *AIChE J.* **66**, 1–23 (2020).
46. Marioni, N. et al. Impact of ion-ion correlated motion on salt transport in solvated ion exchange membranes. *ACS Macro Lett.* **11**, 1258–1264 (2022).
47. Crothers, A. R., Darling, R. M., Kushner, D. I., Perry, M. L. & Weber, A. Z. Theory of multicomponent phenomena in cation-exchange membranes: part III. Transport in vanadium redox-flow-battery separators. *J. Electrochem. Soc.* **167**, 013549 (2020).
48. Fong, K. D., Self, J., McCloskey, B. D. & Persson, K. A. Ion correlations and their impact on transport in polymer-based electrolytes. *Macromolecules* **54**, 2575–2591 (2021).
49. Zhang, H., Cheng, D., Xiang, C. & Lin, M. Tuning the interfacial electrical field of bipolar membranes with temperature and electrolyte concentration for enhanced water dissociation. *ACS Sustain. Chem. Eng.* https://doi.org/10.1021/acssuschemeng.3c00142 (2023).
50. Kaiser, V., Bramwell, S. T., Holdsworth, P. C. W. & Moessner, R. Onsager's Wien effect on a lattice. *Nat. Mater.* **12**, 1033–1037 (2013).

51. Chen, L., Oener, S. Z., Fabrizio, K. & Boettcher, S. W. Design principles for water dissociation catalysts in high-performance bipolar membranes. *Nat. Commun.* **13**, 3846 (2022).
52. Lin, M., Digdaya, I. A. & Xiang, C. Modeling the electrochemical behavior and interfacial junction profiles of bipolar membranes at solar flux relevant operating current densities. *Sustain. Energy Fuels* **5**, 2149–2158 (2021).
53. Bunker, B. C. & Casey, W. H. *The Aqueous Chemistry of Oxides* (Oxford Univ. Press, 2016).
54. Vermaas, D. A., Wiegman, S. & Smith, W. A. Ion transport mechanisms in bipolar membranes for (photo)electrochemical water splitting. *Sustain. Energy Fuels* https://doi.org/10.1039/c8se00118a (2018).
55. Park, H. B., Kamcev, J., Robeson, L. M., Elimelech, M. & Freeman, B. D. Maximizing the right stuff: the trade-off between membrane permeability and selectivity. *Science* **356**, 1138–1148 (2017).
56. Zhang, H. & Geise, G. M. Modeling the water permeability and water/salt selectivity tradeoff in polymer membranes. *J. Memb. Sci.* **520**, 790–800 (2016).
57. Oener, S. Z., Foster, M. J. & Boettcher, S. W. Accelerating water dissociation in bipolar membranes and for electrocatalysis. *Science* **369**, 1099–1103 (2020).
58. Kamcev, J. Reformulating the permselectivity-conductivity tradeoff relation in ion-exchange membranes. *J. Polym. Sci.* **59**, 2510–2520 (2021).
59. Shen, C., Wycisk, R. & Pintauro, P. N. High performance electrospun bipolar membrane with a 3D junction. *Energy Environ. Sci.* **10**, 1435–1442 (2017).
60. Kitto, D. & Kamcev, J. The need for ion-exchange membranes with high charge densities. *J. Memb. Sci.* **677**, 121608 (2023).
61. Xue, J., Liu, L., Liao, J., Shen, Y. & Li, N. UV-crosslinking of polystyrene anion exchange membranes by azidated macromolecular crosslinker for alkaline fuel cells. *J. Memb. Sci.* **535**, 322–330 (2017).
62. McCrory, C. C. L. et al. Benchmarking hydrogen evolving reaction and oxygen evolving reaction electrocatalysts for solar water splitting devices. *J. Am. Chem. Soc.* **137**, 4347–4357 (2015).
63. Xiao, J. et al. Water-fed hydroxide exchange membrane electrolyzer enabled by a fluoride-incorporated nickel-iron oxyhydroxide oxygen evolution electrode. *ACS Catal.* **11**, 264–270 (2021).
64. Li, D. et al. Highly quaternized polystyrene ionomers for high performance anion exchange membrane water electrolysers. *Nat. Energy* **5**, 378–385 (2020).
65. Krivina, R. A. et al. Anode catalysts in anion-exchange-membrane electrolysis without supporting electrolyte: conductivity, dynamics, and ionomer degradation. *Adv. Mater.* **34**, 1–10 (2022).
66. Li, L., Wang, P., Shao, Q. & Huang, X. Recent progress in advanced electrocatalyst design for acidic oxygen evolution reaction. *Adv. Mater.* **33**, 2004243 (2021).
67. Plevová, M., Hnát, J. & Bouzek, K. Electrocatalysts for the oxygen evolution reaction in alkaline and neutral media. A comparative review. *J. Power Sources* **507**, 230072 (2021).
68. Lees, E. W., Mowbray, B. A. W., Parlane, F. G. L. & Berlinguette, C. P. Gas diffusion electrodes and membranes for CO_2 reduction electrolysers. *Nat. Rev. Mater.* **7**, 55–64 (2022).
69. Jeng, E. & Jiao, F. Investigation of CO_2 single-pass conversion in a flow electrolyzer. *React. Chem. Eng.* **5**, 1768–1775 (2020).
70. Blommaert, M. A. et al. Orientation of a bipolar membrane determines the dominant ion and carbonic species transport in membrane electrode assemblies for CO_2 reduction. *J. Mater. Chem. A* **9**, 11179–11186 (2021).
71. Yang, K. et al. Cation-driven increases of CO_2 utilization in a bipolar membrane electrode assembly for CO_2 electrolysis. *ACS Energy Lett.* **6**, 4291–4298 (2021).
72. Eriksson, B. et al. Mitigation of carbon crossover in CO_2 electrolysis by use of bipolar membranes. *J. Electrochem. Soc.* **169**, 034508 (2022).
73. Lees, E. W. et al. Electrolytic methane production from reactive carbon solutions. *ACS Energy Lett.* **7**, 1712–1718 (2022).
74. Li, Y. C. et al. Bipolar membranes inhibit product crossover in CO_2 electrolysis cells. *Adv. Sustain. Syst.* **2**, 1700187 (2018).
75. Salvatore, D. A. et al. Electrolysis of gaseous CO_2 to CO in a flow cell with a bipolar membrane. *ACS Energy Lett.* **3**, 149–154 (2018).
76. Xie, K. et al. Bipolar membrane electrolyzers enable high single-pass CO_2 electroreduction to multicarbon products. *Nat. Commun.* **13**, 3609 (2022).
77. Yan, Z., Hitt, J. L., Zeng, Z., Hickner, M. A. & Mallouk, T. E. Improving the efficiency of CO_2 electrolysis by using a bipolar membrane with a weak-acid cation exchange layer. *Nat. Chem.* **13**, 33–40 (2021).
78. Li, T. et al. Electrolytic conversion of bicarbonate into CO in a flow cell. *Joule* **3**, 1487–1497 (2019).
79. Lees, E. W. et al. Electrodes designed for converting bicarbonate into CO. *ACS Energy Lett.* **5**, 2165–2173 (2020).
80. Lees, E. W., Bui, J. C., Song, D., Weber, A. Z. & Berlinguette, C. P. Continuum model to define the chemistry and mass transfer in a bicarbonate electrolyzer. *ACS Energy Lett.* **7**, 834–842 (2022).
81. Fink, A. G. et al. Electrolytic conversion of carbon capture solutions containing carbonic anhydrase. *J. Inorg. Biochem.* **231**, 111782 (2022).
82. Zhang, Z. et al. Porous metal electrodes enable efficient electrolysis of carbon capture solutions. *Energy Environ. Sci.* **15**, 705–713 (2022).
83. Li, T., Lees, E. W., Zhang, Z. & Berlinguette, C. P. Conversion of bicarbonate to formate in an electrochemical flow reactor. *ACS Energy Lett.* **5**, 2624–2630 (2020).
84. Zhang, Z. et al. Conversion of reactive carbon solutions into CO at low voltage and high carbon efficiency. *ACS Cent. Sci.* **8**, 749–755 (2022).
85. Perry, M. L., Rodby, K. E. & Brushett, F. R. Untapped potential: the need and opportunity for high-voltage aqueous redox flow batteries. *ACS Energy Lett.* **7**, 659–667 (2022).
86. Arevalo-Cid, P., Dias, P., Mendes, A. & Azevedo, J. Redox flow batteries: a new frontier on energy storage. *Sustain. Energy Fuels* **5**, 5366–5419 (2021).
87. Yan, Z. et al. High-voltage aqueous redox flow batteries enabled by catalyzed water dissociation and acid-base neutralization in bipolar membranes. *ACS Cent. Sci.* **7**, 1028–1035 (2021).
88. Chen, R. Redox flow batteries: mitigating cross-contamination via bipolar redox-active materials and bipolar membranes. *Curr. Opin. Electrochem.* **37**, 101188 (2023).
89. Dai, J. et al. A sandwiched bipolar membrane for all vanadium redox flow battery with high coulombic efficiency. *Polymer* **140**, 233–239 (2018).
90. Metlay, A. S. et al. Three-chamber design for aqueous acid-base redox flow batteries. *ACS Energy Lett.* **7**, 908–913 (2022).
91. van Egmond, W. J. et al. Performance of an environmentally benign acid base flow battery at high energy density. *Int. J. Energy Res.* **42**, 1524–1535 (2018).
92. Lu, S., Pan, J., Huang, A., Zhuang, L. & Lu, J. Alkaline polymer electrolyte fuel cells completely free from noble metal catalysts. *Proc. Natl Acad. Sci. USA.* **105**, 20611–20614 (2008).
93. Spendelow, J. S. & Wieckowski, A. Electrocatalysis of oxygen reduction and small alcohol oxidation in alkaline media. *Phys. Chem. Chem. Phys.* **9**, 2654–2675 (2007).
94. Peng, S. et al. A self-humidifying acidic-alkaline bipolar membrane fuel cell. *J. Power Sources* **299**, 273–279 (2015).
95. Li, Q. et al. Theoretical design strategies of bipolar membrane fuel cell with enhanced self-humidification behavior. *J. Power Sources* **307**, 358–367 (2016).

96. Toh, W. L., Dinh, H. Q., Chu, A. T., Sauvé, E. R. & Surendranath, Y. The role of ionic blockades in controlling the efficiency of energy recovery in forward bias bipolar membranes. *Nat. Energy* **8**, 1405–1416 (2023).
97. Sharifian, R., Boer, L., Wagterveld, R. M. & Vermaas, D. A. Oceanic carbon capture through electrochemically induced in situ carbonate mineralization using bipolar membrane. *Chem. Eng. J.* **438**, 135326 (2022).
98. Iizuka, A. et al. A process for capturing CO_2 from the atmosphere. *Ind. Eng. Chem. Res.* **4**, 1–11 (2022).
99. Eisaman, M. D., Alvarado, L., Larner, D., Wang, P. & Littau, K. A. CO_2 desorption using high-pressure bipolar membrane electrodialysis. *Energy Environ. Sci.* **4**, 4031–4037 (2011).
100. Zhu, P. et al. Continuous carbon capture in an electrochemical solid-electrolyte reactor. *Nature* **618**, 959–966 (2023).
101. Zhang, Z. et al. Cement clinker precursor production in an electrolyser. *Energy Environ. Sci.* **15**, 5129–5136 (2022).
102. Zhang, Z. B., Mowbray, B. A. W., Parkyn, C. T. E., Kim, Y. & Berlinguette, C. P. Electrolytic cement clinker production sustained through orthogonalization of ion vectors. Preprint at *ChemRxiv* https://doi.org/10.26434/chemrxiv-2023-0zcw9 (2023).
103. Chen, J. G. et al. Beyond fossil fuel–driven nitrogen transformations. *Science* **360**, eaar6611 (2018).
104. van Linden, N., Bandinu, G. L., Vermaas, D. A., Spanjers, H. & van Lier, J. B. Bipolar membrane electrodialysis for energetically competitive ammonium removal and dissolved ammonia production. *J. Clean. Prod.* **259**, 120788 (2020).
105. Dong, H., Laguna, C. M., Liu, M. J., Guo, J. & Tarpeh, W. A. Electrified ion exchange enabled by water dissociation in bipolar membranes for nitrogen recovery from source-separated urine. *Environ. Sci. Technol.* **56**, 16134–16143 (2022).
106. Sabatino, F., Gazzani, M., Gallucci, F. & Van Sint Annaland, M. Modeling, optimization, and techno-economic analysis of bipolar membrane electrodialysis for direct air capture processes. *Ind. Eng. Chem. Res.* **61**, 12668–12679 (2022).
107. Zhao, S. et al. Engineering antifouling reverse osmosis membranes: a review. *Desalination* **499**, 114857 (2021).
108. Anis, S. F., Hashaikeh, R. & Hilal, N. Reverse osmosis pretreatment technologies and future trends: A comprehensive review. *Desalination* **452**, 159–195 (2019).
109. Calado, G. & Castro, R. Hydrogen production from offshore wind parks: current situation and future perspectives. *Appl. Sci.* **11**, e202200372 (2021).
110. Han, J. H. Exploring the interface of porous cathode/bipolar membrane for mitigation of inorganic precipitates in direct seawater electrolysis. *ChemSusChem* **15**, e202200372 (2022).
111. Han, J. H. et al. Direct seawater electrolysis via synergistic acidification by inorganic precipitation and proton flux from bipolar membrane. *Chem. Eng. J.* **429**, 132383 (2022).
112. Han, J. H. Complete suppression of dispersed inorganic precipitates in reverse electrodialysis via seawater acidification. *Ind. Eng. Chem. Res.* **61**, 9165–9170 (2022).
113. Andreeva, M. A. et al. Mitigation of membrane scaling in electrodialysis by electroconvection enhancement, pH adjustment and pulsed electric field application. *J. Memb. Sci.* **549**, 129–140 (2018).
114. Davis, J. T., Qi, J., Fan, X., Bui, J. C. & Esposito, D. V. Floating membraneless PV-electrolyzer based on buoyancy-driven product separation. *Int. J. Hydrogen Energy* 1224–1238, https://doi.org/10.1016/j.ijhydene.2017.11.086 (2017).
115. Dresp, S., Dionigi, F., Klingenhof, M. & Strasser, P. Direct electrolytic splitting of seawater: opportunities and challenges. *ACS Energy Lett.* **4**, 933–942 (2019).
116. Blommaert, M. A., Verdonk, J. A. H., Blommaert, H. C. B., Smith, W. A. & Vermaas, D. A. Reduced ion crossover in bipolar membrane electrolysis via increased current density, molecular size and valence. *ACS Appl. Energy Mater.* **3**, 5804–5812 (2020).
117. Dionigi, F., Reier, T., Pawolek, Z., Gliech, M. & Strasser, P. Design criteria, operating conditions, and nickel-iron hydroxide catalyst materials for selective seawater electrolysis. *ChemSusChem* **9**, 962–972 (2016).
118. Rossi, R. et al. Using a vapor-fed anode and saline catholyte to manage ion transport in a proton exchange membrane electrolyzer. *Energy Environ. Sci.* **14**, 6041–6049 (2021).
119. Katzenberg, A., Angulo, A., Kusoglu, A. & Modestino, M. A. Impacts of organic sorbates on the ionic conductivity and nanostructure of perfluorinated sulfonic-acid ionomers. *Macromolecules* **54**, 5187–5195 (2021).
120. Geise, G. M. et al. Water purification by membranes: the role of polymer science. *J. Polym.* **48**, 1685–1718 (2010).
121. Mayerhöfer, B. et al. On the effect of anion exchange ionomer binders in bipolar electrode membrane interface water electrolysis. *J. Mater. Chem. A* **9**, 14285–14295 (2021).
122. Chen, Y. et al. High-performance bipolar membrane development for improved water dissociation. *ACS Appl. Polym. Mater.* **2**, 4559–4569 (2020).
123. Li, D. et al. Durability of anion exchange membrane water electrolyzers. *Energy Environ. Sci.* **14**, 3393–3419 (2021).
124. Krivina, R. A. et al. Three-electrode study of electrochemical ionomer degradation relevant to anion-exchange-membrane water electrolyzers. *ACS Appl. Mater. Interfaces* **14**, 18261–18274 (2022).
125. Lindquist, G. A. et al. Performance and durability of pure-water-fed anion exchange membrane electrolyzers using baseline materials and operation. *ACS Appl. Mater. Interfaces* **13**, 51917–51924 (2021).
126. Lindquist, G. A. et al. Oxidative instability of ionomers in hydroxide-exchange-membrane water electrolyzers. *Energy Environ. Sci*. https://doi.org/10.1039/d3ee01293j (2023).
127. Maurya, S. et al. On the origin of permanent performance loss of anion exchange membrane fuel cells: electrochemical oxidation of phenyl group. *J. Power Sources* **436**, 226866 (2019).
128. Kusoglu, A., Calabrese, M. & Weber, A. Z. Effect of mechanical compression on chemical degradation of Nafion membranes. *ECS Electrochem. Lett.* **3**, F33 (2014).
129. Cullen, D. A. et al. New roads and challenges for fuel cells in heavy-duty transportation. *Nat. Energy* **6**, 462–474 (2021).
130. Curtin, D. E., Lousenberg, R. D., Henry, T. J., Tangeman, P. C. & Tisack, M. E. Advanced materials for improved PEMFC performance and life. *J. Power Sources* **131**, 41–48 (2004).
131. Pianca, M., Barchiesi, E., Esposto, G. & Radice, S. End groups in fluoropolymers. *J. Fluor. Chem.* **95**, 71–84 (1999).
132. Danilczuk, M., Schlick, S. & Coms, F. D. Cerium(III) as a stabilizer of perfluorinated membranes used in fuel cells: In situ detection of early events in the ESR resonator. *Macromolecules* **42**, 8943–8949 (2009).
133. Gubler, L. & Koppenol, W. H. Kinetic simulation of the chemical stabilization mechanism in fuel cell membranes using cerium and manganese redox couples. *J. Electrochem. Soc.* **159**, B211–B218 (2011).
134. Trogadas, P., Parrondo, J. & Ramani, V. Degradation mitigation in polymer electrolyte membranes using cerium oxide as a regenerative free-radical scavenger. *Electrochem. Solid-State Lett.* **11**, B113 (2008).
135. Collette, F. M., Lorentz, C., Gebel, G. & Thominette, F. Hygrothermal aging of Nafion®. *J. Memb. Sci.* **330**, 21–29 (2009).
136. Arthurs, C. & Kusoglu, A. Compressive creep of polymer electrolyte membranes: a case study for electrolyzers. *ACS Appl. Energy Mater.* **4**, 3249–3254 (2021).

137. Sadeghi Alavijeh, A., Khorasany, R. M. H., Habisch, A., Wang, G. G. & Kjeang, E. Creep properties of catalyst coated membranes for polymer electrolyte fuel cells. *J. Power Sources* **285**, 16–28 (2015).
138. Xu, Z. et al. Continuous ammonia electrosynthesis using physically interlocked bipolar membrane at 1000 mA cm^{-2}. *Nat. Commun.* **14**, 1619 (2023).
139. Rajesh, A. M., Chakrabarty, T., Prakash, S. & Shahi, V. K. Effects of metal alkoxides on electro-assisted water dissociation across bipolar membranes. *Electrochim. Acta* **66**, 325–331 (2012).
140. Wang, Q., Wu, B., Jiang, C., Wang, Y. & Xu, T. Improving the water dissociation efficiency in a bipolar membrane with amino-functionalized MIL-101. *J. Memb. Sci.* **524**, 370–376 (2017).
141. Yan, Z. et al. The balance of electric field and interfacial catalysis in promoting water dissociation in bipolar membranes. *Energy Environ. Sci.* **11**, 2235–2245 (2018).
142. Ge, Z. et al. High-performance bipolar membrane for electrochemical water electrolysis. *J. Memb. Sci.* **656**, 120660 (2022).
143. Hohenadel, A. et al. Electrochemical characterization of hydrocarbon bipolar membranes with varying junction morphology. *ACS Appl. Energy Mater.* **2**, 6817–6824 (2019).
144. Hohenadel, A., Gangrade, A. S. & Holdcroft, S. Spectroelectrochemical detection of water dissociation in bipolar membranes. *ACS Appl. Mater. Interfaces* **13**, 46125–46133 (2021).
145. Kim, B. S. et al. Bipolar membranes to promote formation of tight ice-like water for efficient and sustainable water splitting. *Small* **16**, 2002641 (2020).
146. McDonald, M. B. & Freund, M. S. Graphene oxide as a water dissociation catalyst in the bipolar membrane interfacial layer. *ACS Appl. Mater. Interfaces* **6**, 13790–13797 (2014).

Acknowledgements

This material is partially based on work performed within the Liquid Sunlight Alliance, which is supported by the US Department of Energy, Office of Science, Office of Basic Energy Sciences, Fuels from Sunlight Hub under award number DE-SC0021266 as well as the US Department of Energy under contract number DE-AC02-05CH11231. J.C.B. was supported in part by a fellowship award under contract FA9550-21-F-0003 through the National Defense Science and Engineering Graduate (NDSEG) fellowship program, sponsored by the Army Research Office (ARO). T.N.S. acknowledges funding from the National Science Foundation Graduate Research Fellowship (NSFGRFP) under grant number DGE 2146752. E.W.L. acknowledges funding from the National Science and Engineering Research Council of Canada (NSERC). S.W.B. and L.C. acknowledge support from the US Office of Naval Research, grant N00014-20-1-2517.

Author contributions

J.C.B. and A.Z.W. supervised the project. J.C.B. conceived of the article, coordinated authors, and combined and unified author contributions. All authors contributed to discussing, commenting on, writing, and revising the manuscript.

Competing interests

The authors declare no competing interests.

Additional information

Correspondence and requests for materials should be addressed to Justin C. Bui or Adam Z. Weber.

Peer review information *Nature Chemical Engineering* thanks Gaohong He, Tongwen Xu and Nana Zhao for their contribution to the peer review of this work.